# Numerical Investigation of Tuned Liquid Damper Performance Attached to a Single Degree of Freedom Structure

# Numerical Investigation of a Tuned Liquid Damper Performance Attached to a Single Degree of Freedom Structure

By Omar Al Jamal, B.Sc.

A Thesis

Submitted to the School of Graduate Studies

In Partial Fulfillment of the Requirements

For The Degree

Master of Applied Science

McMaster University

September 2015

MASTER OF APPLIED SCIENCE (2015) McMaster University

(Mechanical Engineering) Hamilton, Ontario

TITLE: Numerical Investigation of a Tuned Liquid Damper Performance Attached to a Single Degree of Freedom Structure

AUTHOR: Omar Al Jamal, B.Sc. (Qatar University, Doha, Qatar)

SUPERVISOR: Dr. Mohamed .S. Hamed

NUMER OF PAGES: 93

## Abstract

Tuned liquid dampers (TLDs) are increasingly being used as dynamic vibration absorbers to minimize the vibration of structures. A tuned liquid damper is a tank filled with a liquid. When attached to a structure, the liquid sloshing action inside the TLD dampens and absorbs part of the energy given to the structure. The difficulty in designing TLDs arises from its nonlinear response (behavior), which requires a detailed understanding of the sloshing motion inside the TLD. An in-house numerical algorithm has been developed to investigate and understand liquid sloshing motion inside TLDs and to evaluate the TLD damping performance when coupled with a vibrating Single Degree of Freedom (SDOF) structure. The model is based on the finite-difference method. The Volume of Fluid method has been used to reconstruct the liquid free surface. The Continuum Surface Force model has been used to model and resolve the discontinuity accompanied with wave breaking that might take place at the liquid surface. All dynamic stresses on the free surface have been taken into consideration to evaluate wave breaking. No linearization assumptions have been used in solving the Navier-Stokes equations. The developed numerical model incorporates the interaction between the structure dynamics and the TLD. In this study, the structure has been assumed as a SDOF system and its dynamic response has been calculated using the Duhamel integral method.

The model has been validated against experimental data with and without the structure. Good agreement was obtained between the numerical and the experimental results.

An extensive parametric study has been carried out using the developed numerical model to investigate the effect of TLD-structure frequency ratio ($f_{TLD}/f_s$), external excitation amplitude-TLD length ratio (A/L) and external excitation frequency ratio ($f_{TLD}/f_e$) on the TLD damping performance. A new parameter defined as the Energy Dissipation Factor (EDF) has been introduced to quantify the TLD damping performance. The present results have been used to develop a useful design empirical correlation of the damping effect of the TLD as function of $f_{TLD}/f_s$, A/L and $f_{TLD}/f_{e.}$ .

***This thesis is dedicated to my beloved parents and wife.***

*For their endless love, support and encouragement*

## Acknowledgements

I would like to express the deepest appreciation to my supervisor Dr. Mohamed Hamed, who has the attitude and substance of a genius: he continually and convincingly conveyed a spirit of adventure in regards to research, and an excitement in regards to mentorship. Without his guidance and persistent help this dissertation would not have been accomplished.

I place on record my special thanks to Dr.Tarek Oda, my co-supervisor and the author of the numerical algorithm that was used in this study. His outstanding guidance and support during the course of this research enriched my knowledge and enlightened me extensively.

I thank profusely all my friends and staff of the Mechanical Engineering Department for their support and encouragement. I specially thank Mr. Mohamed Yasser, Mr. Ahmed Ashour, Mr. Naief Almalki, Mr. Mohamed Hamda and Mr. Hasan Rafi for their constructive discussions, support and friendship.

Last but certainly not least, I would like to thank my family for their endless support and understanding. I say Thank You to my father, who encouraged me to take a hands-on approach to solving problems, to my mother for her reassuring words and limitless faith in me and to my wife for her unyielding sacrifices and immeasurable support during this study.

# Table of Contents

# List of Tables

# List of Figures

## Nomenclature

| | | |
|---|---|---|
| A | Amplitude of external dynamic excitation | [m] |
| $M_s$ | Generalized mass of the equivalent SDOF model | [Kg] |
| $m_1$ | Absorber mass | [Kg] |
| $C_s$ | Generalized damping coefficient | [N.s/m] |
| $K_s$ | Generalized stiffness coefficient | [N/m] |
| $F_e$ | External excitation force | [N] |
| $\vec{V}$ | Generalized velocity vector | [m/s] |
| $u$ | The fluid flow velocity component in x-direction | [m/s] |
| $v$ | The fluid flow velocity component in y-direction | [m/s] |
| $g_x$ | Horizontal acceleration | [m/s$^2$] |
| $g_y$ | Gravitational acceleration | [m/s$^2$] |
| $\eta$ | Free surface elevation over the nominal fluid height | [m] |
| $\rho$ | Fluid density | [kg/m$^3$] |
| $\mu$ | Fluid dynamic viscosity | [N.s/m$^2$] |
| $\tau$ | Fluid flow stress | [N/m$^2$] |
| $\sigma$ | Surface tension | [N/m] |
| $\omega$ | Excitation angular frequency | [rad. /s] |
| $\zeta$ | Damping ratio | [-] |
| $\vec{F}_{sv}$ | The Volume force | [N/m$^3$] |
| $\vec{F}_{sa}$ | The surface force upon an interfacial area | [N/m$^2$] |
| $\vec{F}_b^{\,n}$ | The body force at the pervious time step | [N/m$^3$] |
| $F_{TLD}$ | Damping Force | [N] |

| | | |
|---|---|---|
| h | Height of the initial flat free surface | [m] |
| H | The TLD tank Height | [m] |
| L | The TLD tank length | [m] |
| W | The TLD tank width | [m] |
| $p$ | pressure | [N/m$^2$] |
| t | time | [Sec.] |
| $x, y$ | Cartesian coordinates | [m] |
| C* | Courant time Multiplier | [-] |
| $f_{TLD}/f_s$ | Structure frequency ratio | [-] |
| $f_{TLD}/f_e$ | External Excitation Frequency Ratio | [-] |
| A/L | External Excitation Amplitude Ratio | [-] |
| FFT | Fast Fourier Transform | [-] |
| EDR | Energy Dissipation Ratio | [-] |
| EDF | Energy Dissipation Factor | [-] |

# 1 Chapter 1: Introduction

In our modern era, buildings are mainly constructed to be taller and increasingly flexible, which make them very sensitive to external excitations. Controlling the dynamic response caused by of these excitations has become extremely important to the civil structure community. For tall buildings, wind forces cause considerable vibrations. Although these vibrations might not affect the building structural integrity, they may cause huge discomfort to people living in the top floors of the building. Several auxiliary damping systems can be employed to reduce wind-induced motions of tall buildings. As illustrated in Figure 1.1, damping systems can generally be categorized into two main types: passive dampers and active dampers; The main difference between these two types of dampers is that the later requires external power supply to operate while the former depends on the use of energy absorbing materials and elements to mitigate the vibration. The present research is focused on the use of Tuned Liquid Dampers (TLDs), which fall under the category of passive dampers.

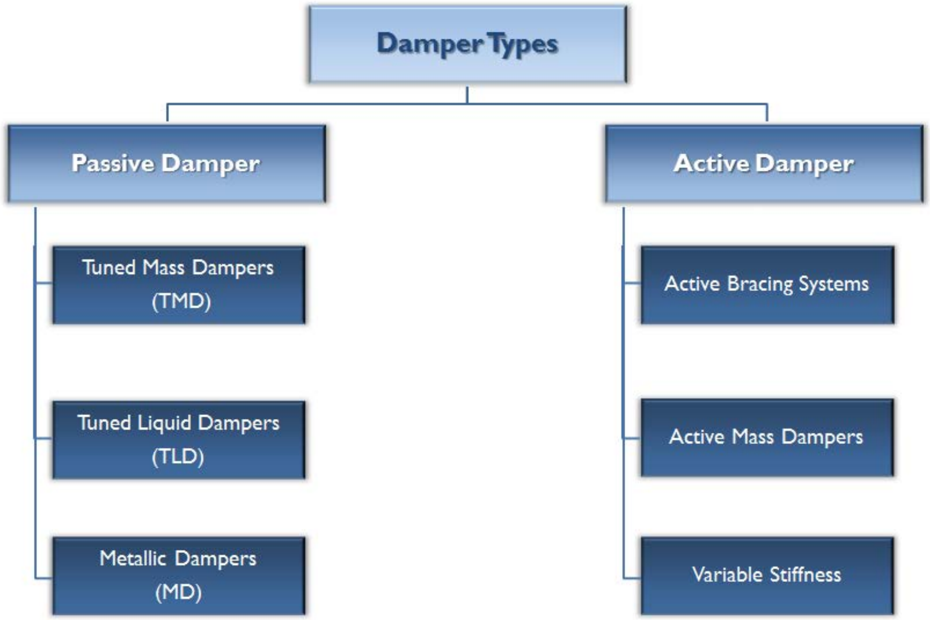


**Figure 1.1: Classification of Dampers**

## 1.1 Passive Dynamic Vibration Absorbers

The simplicity and reliability of passive dampers have made them the preferred means for structural motion control. The main function of these devices is to absorb a portion of the external excitation energy such as wind or earthquake. Currently, the most commonly used passive devices are the tuned mass dampers (Kareem et al., 1999). A schematic representation of a simple tuned mass damper (TMD) is presented in Figure 1.2. A TMD consists of a mass, a spring, and a dashpot. The concept of operation of a TMD is that its mass ($m_1$) produces an antiphase force with the external excitation, which absorbs part of the energy imparted into the structure.

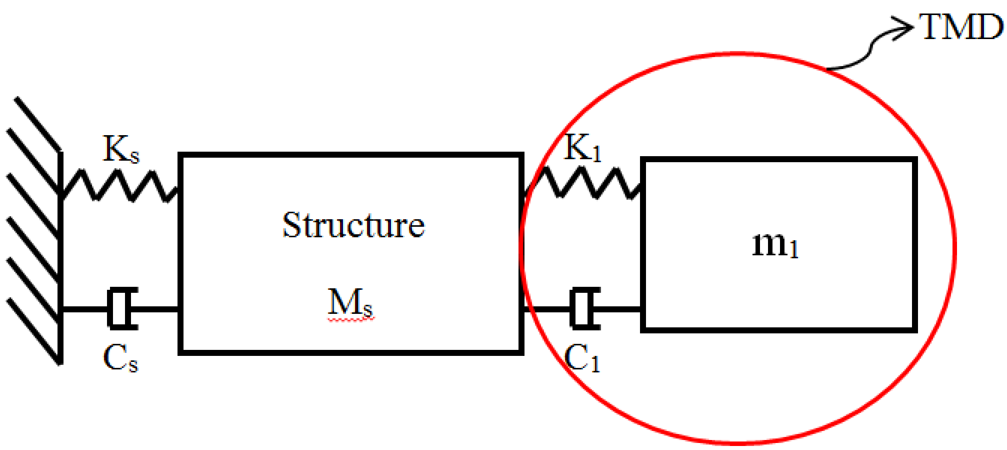


**Figure 1.2: Schematic of a Tuned Mass Damper (TMD)**

Two popular examples of the TMD are found in Citicorp Center in New York, which was built in 1981 (Soong and Dargush, 1997), and the Taipei 101 building in Taiwan, which was built in 2004. Figure 1.3 shows a schematic of the TMD used in the Taipei 101 building.

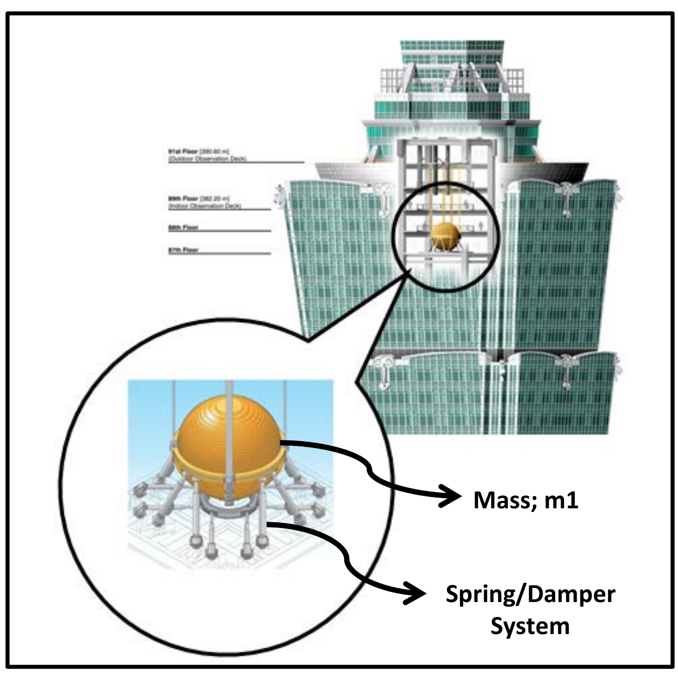


**Figure 1.3: Taipei 101 Building TMD**

### 1.2 Tuned Liquid Dampers (TLDs)

A Tuned liquid damper (TLD) is a tank partially filled with a liquid, usually water. Figure 1.4 shows a schematic of a typical TLD with length, L, width W, height H, and initial water height, h.

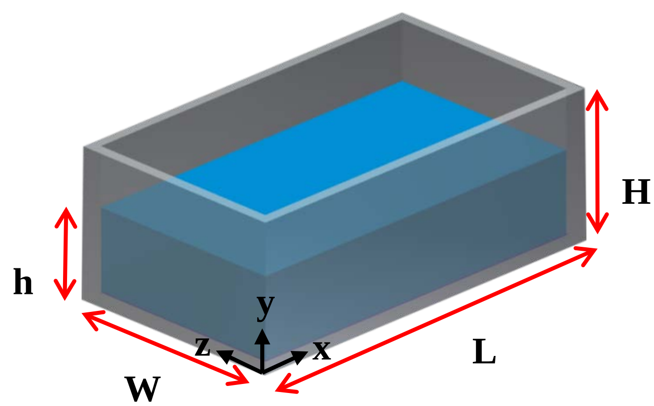


**Figure 1.4: Tuned Liquid Damper (TLD)**

The concept of the tuned liquid dampers is very similar to that of the TMD. In the TMD the secondary mass is a solid mass while in the TLD, the liquid inside the tank acts as the secondary mass. Figure 1.5 shows a schematic of the simple vibration model a TLD attached to a structure. $M_s$, $K_s$ and $C_s$ are the structure mass, spring coefficient, and damping coefficient, respectively.

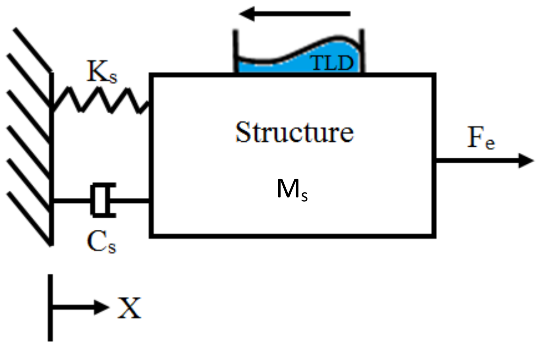


**Figure 1.5: The vibration model of a Tuned Liquid Damper (TLD) attached to a structure**

The idea of using the TLD as damping devise was proposed by Frahm in the early 1900s (Soong and Dargush, 1997). At that time, the TLD was primarily used for marine applications to stabilize marine vessels against rocking and rolling sea motion (Matsuuara et al., 1986). In the mid-1980s, this idea started to get attention in civil engineering structures to reduce vibration resulting from earthquakes and wind excitations. In 1984, Bauer (Soong and Dargush, 1997) proposed a rectangular tank full of two immiscible liquids to be used a vibration damper while the damping effect is due to the motion of the interface. In 1989, Modi and Welt (Soong and Dargush, 1997) were among the first researchers who suggested the TLDs in buildings to reduce overall response due to wind or earthquakes. Later on, this technique was modified by Fujino et al. (1992), Wakahara et al. (1992), Wakahara (1993), Reed et al. (1998) and Tait et al. (2005) to stabilize high-rise buildings.

Due to the external excitation, the water inside the TLD sloshes creating a wave as shown in Figure 1.6, which in turns, produces an inertia force on the structure that approximately anti-phase to the excitation force, thereby, reducing the structural sway. As such, the attachment of a TLD to a structure modifies the structure response in a way similar to increasing the structure effective damping. The energy dissipation occurs due to viscous dissipation in the boundary layer at the walls and the bottom of the tank, as well as from free surface breaking.

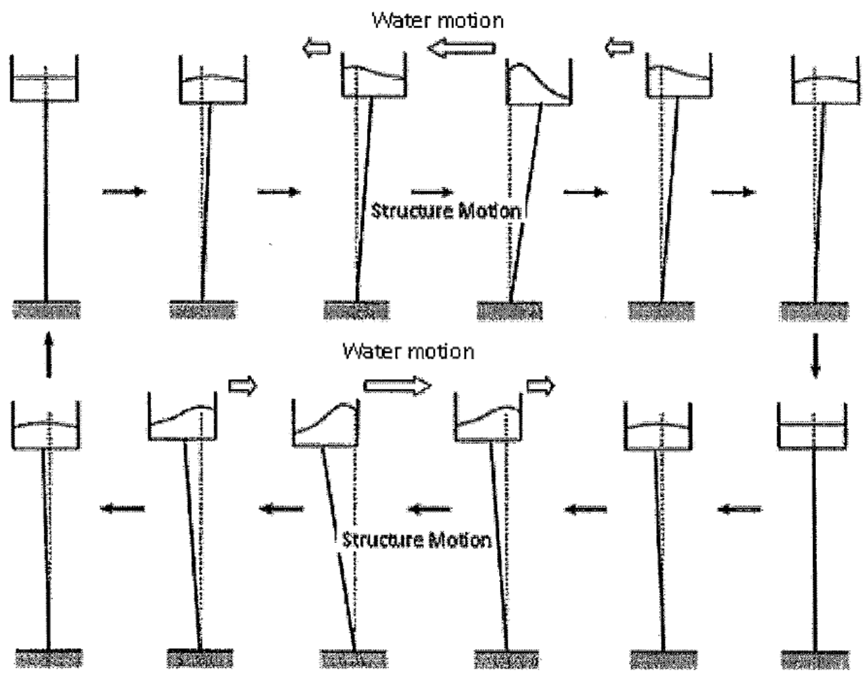


**Figure 1.6: Schematic of TLD principles [Yamamoto and Kawahara, 1999]**

The attractiveness of TLDs lies in their low cost, low maintenance requirements, and simple design compared to other vibration dampers. Moreover, TLDs can be used as water tanks for building, either to be used for regular water supply or for fire fitting emergencies.

However, unlike TMDs, the response of a TLD is in general highly nonlinear and naturally complex due to the liquid sloshing motion. This complexity is also attributed to wave breaking that could occur at the free surface, depending on the liquid height, tank dimensions, and level of the external excitation. Therefore, TLDs can be broadly classified into two types: (1) shallow-water (SW) TLDS and (2) deep-water (DW) TLDS. This classification is based on the ratio of the water depth to the tank length. If the liquid depth is around 10-12 % (Dalrymple and Dean, 1991) of the tank length, the TLD is considered a SW damper. In shallow water dampers, the damping occurs primarily due to viscous dissipation at the tank walls and due to wave breaking at the liquid interface. Therefore, SW TLDS tend to have a high damping capability. However, SW TLDS require large surface areas for installation. On the other hand, damping in DP TLDS occurs only due to viscous dissipation and hence DW TLDS are characterized by lower damping. This fact led many researchers, such as Fujino et al., 1988, Tamura et al., 1995, Noji et al., 1988; Warnitchani and Pinkaew, 1998; Kaneko and Ishikawa, 1999; Tait M. J., 2004; Hemelin, 2007 to investigate several techniques to enhance the damping capability of DW TLDs. . Some of these techniques include the use of surface contaminants and screens.

### 1.3 Tuned Liquid damper (TLD) Implementations

As indicated before, due to their simple design and low maintenance, many water tanks already available in tall buildings have been used as TLDs to suppress vibration due to wind. The first TLD application is in the Yokohama Marine Tower in Japan, which was built in 1987. The TLDs used in this building are shown in the Figure 1.8.

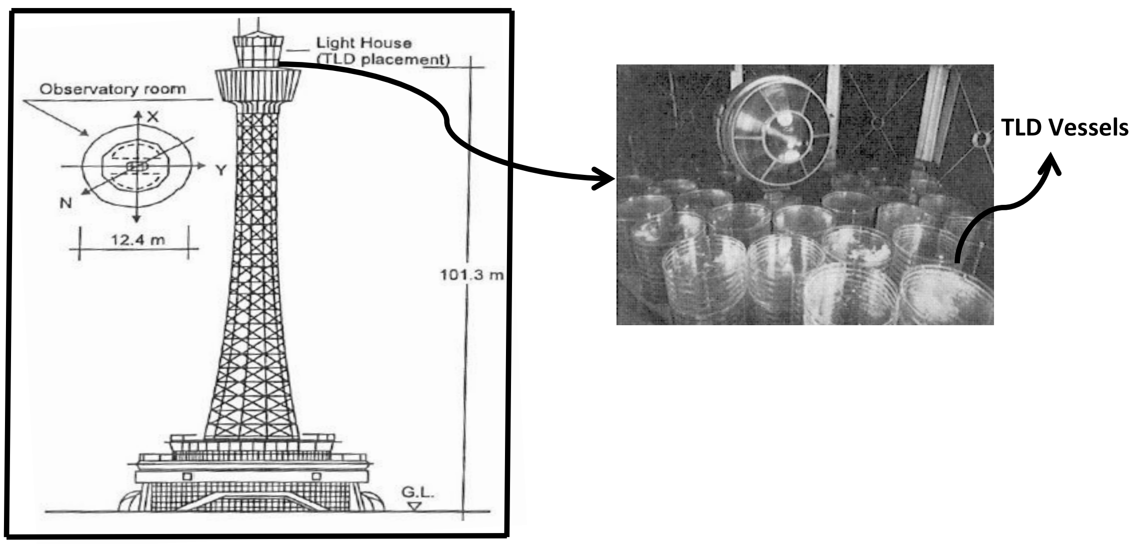


**Figure 1.7: Yokohama Marine Tower [Soong and Dargush, 1997]**

Two more recent examples of towers outfitted with TLDs are the One King West Tower in Toronto, Canada, which was completed in 2005 and the One Rincon Hill Tower in San Francisco, U.S.A, which was completed in 2009, see Figure 1.9.

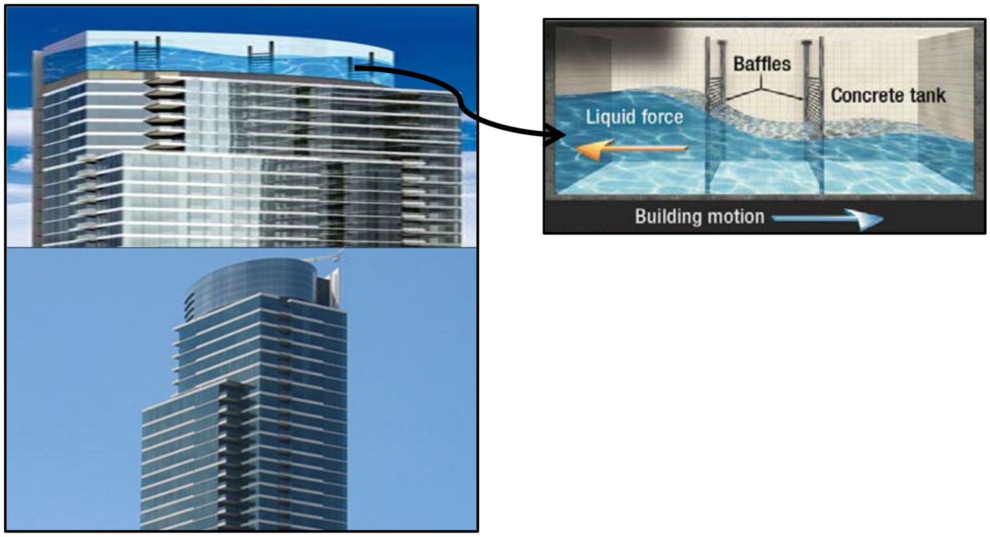


**Figure 1.8: One Rincon Hill Tower**

# 2 Chapter 2: Literature Review

Since the 1980s, TLDs have gain significant attention as an attractive research topic. Throughout this section, the experimental and numerical studies that have conducted on TLDs are reviewed.

## 2.1 Experimental Work Carried out on TLDs

In the early research work on TLDs, it was very difficult to predict and study the phenomenon of liquid sloshing inside the TLD by theoretical analysis. Consequently, experimental studies were carried out to gain a better understanding of the nature of liquid motion inside the TLD.

The earliest experimental studies on TLDs were carried out by Modi and Welt (1987) and Fujino et al. (1988). Fujino et al. investigated the effects of liquid viscosity, roughness of container bottom, air gap between the liquid and tank roof and container size on the overall TLD damping performance. Their TLDs were cylindrical containers. Modi and Welt (1987) performed an experimental and an analytical study on a nutation damper (annular tank).

Many experimental investigations have been carried out on rectangular TLDs. Fujino et al. (1992); Sun and Fujino (1994) and Sun et al. (1995) studied the performance of rectangular TLDs using on the shallow water wave theory. They considered small vibration amplitudes so that wave breaking did not take place inside their TLDs. Similar experiments were carried out by Koh et al. (1994) who considered earthquake-type excitations as opposed to sinusoidal excitations utilized in previous studies.

Reed et al. (1998) experimentally investigated the TLD behavior under large amplitude excitations and compared their results with a numerical model that they developed using the non-linear shallow-water wave equations. Chang and GU (1999) investigated control parameters of rectangular TLDs installed on a tall building that was exposed to vibrate due to vortex excitation.

Tait (2004) conducted many of experimental and numerical cases to investigate the efficiency and robustness of structure-TLD systems for various response amplitudes, tuning ratios, water depths to tank length ratios and screen solidity ratios. The nonlinear numerical model based on shallow water wave theory is found to accurately predict the response for a number of structure-TLD systems. The model is verified for different parameters including different tank geometries, fluid depths and damping screen solidity ratios.

Li and Wang (2004) experimentally and theoretically investigated the performance of multiple TLDs installed on tall buildings and high-rise structures that were excited due to earthquakes.

Akyildiz and Unal (2005) investigated pressure distributions at different locations in the TLD tank and 3D effects on liquid sloshing. For this reason, an experimental setup was designed to study the non-linear behavior and damping characteristics of liquid sloshing in partially filled 3D rectangular tanks with various liquid levels.

P.K. Panigrahy et al. (2009) conducted a series of experiments in a TLD to estimate the pressure developed on the tank walls and the free surface displacement of water from the mean static level. The pressure at different locations and different liquid depths has been measured and the pressure time plots were reported. The experiments were carried out with and without baffles placed inside the TLD.

## 2.2 Numerical Modelling of TLD

Numerous numerical models have been developed and used to assess liquid sloshing behavior inside TLDs. Early studies using analytical and numerical models were carried out under the assumption of moderate amplitudes of sloshing so that no wave breaking was expected. These models represent extensions of the classical theories developed by Airy and Boussinesq for shallow water tanks (Soong and Dargush, 1997). Housner (1957, 1963) introduced the first numerical modeling of sloshing liquids and his model considered only the linearized response.

Generally, the analytical and numerical models have been developed based on two main theories: the potential-flow theory which considers incompressible, inviscid, and irrotational flows; and the shallow-water wave theory which solves the nonlinear Navier Stokes equations under the assumption of relatively low-wave height compared to the mean depth of the liquid layer inside the tank.

The majority of the numerical models reported in the literature utilized the potential flow theory [Nakayama and Washizu (1981); Nakayama (1983); Ohyama and

Fuji (1989); Tosaka and Sugino, 1991; Faltinsen et al., 2000; Faltinsen and Timokha, 2001, 2002; Bredmose et al., 2003]. In the last ten years, there has been an increasing interest in the study of sloshing phenomena in under depth conditions [Reed et al., 1998; Shimizu and Hayama, 1987; Sun, 1991; Faltinsen and Timokha, 2002; Hill, 2003; Tait et al., 2005; Faltinsen, 2005; Lugnil et al., 2006, 2010].

Lepelletier and Raichlen (1988); Okomoto and Kawahara (1990); Chen et al. (1996) conducted studies under large external excitation amplitudes. Sun et al. (1989), Sun et al. (1992), Sun and Fujino (1994), Sun et al. (1995) improved a nonlinear model by joining the shallow water theory with the boundary layer theory where the effect of the viscous stresses was dominant in the vicinity of the obstacle walls. This model was developed to consider the effect of wave breaking by introducing two empirical coefficients.

Another nonlinear numerical model was proposed by Modi and Seto (1997). This model accounted for the effect of wave dispersion (wave splitting up by frequency) and the boundary layer at the walls as well as a floating particle interaction at the free surface. A 3-D numerical model has been developed by Wu et al. (1998) to investigate the liquid sloshing inside TLD tanks based on the potential flow theory.

Warnitchai and Pinkaew (1998) proposed a numerical model of TLDs that included the non-linear effects of flow-dampening devices. In 1999, an analytical model that was able to consider the effect of submerged nets on the TLD behavior based on the shallow water wave theory was proposed by Kaneko and Ishikawa (1999).

Faltinsen (1978, 2000) developed a numerical model to study liquid sloshing inside a TLD based on the boundary element model (BEM) and the potential flow theory. Using the BEM, Nakayama and Washizu (1981) studied liquid sloshing inside a rectangular tank subjected to surge, heave, and pitch motions.

Zang, Xue and Kurita (2000) developed a numerical model by using a linearized form of the Navier-Stokes equations by neglecting the convective acceleration terms. This model was used to investigate sloshing motion inside a TLD. They considered only the case of small amplitude external excitations and external excitations with frequency away from the natural frequency of the TLD. Banerji et al. (2000) studied the effectiveness of the important TLD parameters based on the model introduced by Sun et al. (1992).

Li et al. (2002) solved the continuity and momentum fluid equations for a shallow liquid layer using the finite element method. They simplified the three dimensional problem into a one-dimensional problem.

Frandsen (2005) developed a fully nonlinear 2-D σ-transformed finite difference model based on the inviscid flow equations in rectangular tanks. This model was not able to capture either the damping effects of the liquid or the shallow-water wave behavior.

A numerical model was developed by Marivani (2009) to investigate the 2-D viscous, incompressible flow inside a TLD without imposing any linearization assumptions. However, Marivani's model did not account for all dynamic stresses at the free surface; therefore it can only be used under conditions that do not lead to wave breaking at the liquid interface.

Antuono et al. (2012) developed a numerical modal that was capable of describing the sloshing motion generated by a general two dimensional force by using Boussinesq-type depth-averaged equations.

In 2013, Bouscasse et al. carried out a numerical and an experimental analysis of sloshing motion inside a TLD. Their numerical simulations were performed using the smoothed particle hydrodynamics (SPH) model. SPH model is a meshless Lagrangian method which proves to be well suited for simulating complex fluid dynamics Antuono et al. (2010). The method relies on the idea of dividing the flow region into particles instead of meshes thus no boundary conditions are required at the free surface and consequently can capture phenomena such as wave breaking Monaghan (1988).

Antuono et al. (2014) proposed a new model that accounted for wave breaking in side rectangular tanks under shallow-water conditions. The model was obtained by applying Fourier analysis to Boussinesq-type equations and using an approximate analytical solution of the vorticity generated by wave breaking.

The models mentioned above have limited applicability. These models approximated the location of the free surface by considering the liquid layer to be shallow and hence assumed that the free surface does not significantly deform. However, experimental studies indicated that the liquid interface inside the TLD could undergo sever deformations that could lead to wave breaking; under some operating conditions. Therefore, different types of models that must be able to: (1) account for all physical effects (inertia and viscosity), and (2) solve the moving boundary problem under conditions leading to small and large interfacial deformations. As a result, a different class of numerical models were developed addressing these needs. In the first attempt, the Marker-And-Cell (MAC) method was used by Harlow and Welch, 1965; Chan and Street, 1970; Lemos, 1992 and McKee et al., 2008]. The MAC method follows the moving free surface by tracking the movement of a set of imaginary markets. The free surface cell is defined as the cell that includes at least one marker while its neighbor cells do not include one. The MAC method has a disadvantage of being computationally expensive because it requires too much storage memory to store the coordinates of each particle moving with the fluid per cycle.

This problem was solved by using the Volume of fluid (VOF) method. The VOF method [Hirt and Nichols, 1981; Nichols et al., 1980; Reed et al., 1998; Koth et al., 1996; Lin et al., 1997; Rider, 1998; Bassman, 2000; Min Soo Kim, 2003; Babaei et al., 2006; Lin, 2007] was shown to be more flexible and efficient in treating complicated free boundary configurations. In this method, it is customary to use only one value for each dependent variable defining the liquid state, subsequently a volume fraction; F, of value equal to 1 would correspond to a cell full of liquid, while a value of “0” indicate that the cell contains no liquid. Cells with F values between “0” and “1” must then contain a free surface. Since all the liquid cells have the same factor defining their values, the requirement for storage memory is less, thus the VOF method has a lower computational cost.

Floryan and Rasmussen (1989) reviewed various modelling techniques of moving boundary problems including algorithms that track the moving boundary using fixed grids (Eulerian scheme), adaptive grids (Lagrangian scheme) and arbitrary Lagrangian – Eulerian formulations. However, these schemes differ in the manner in which the fluid elements are moved to the next positions after their new velocities have been computed. In the Lagrangian case, the computational grid simply moves with the computed element velocities; while in an Eulerian or Arbitrary Lagrangian - Eulerian calculation, it is necessary to compute the flow of fluid through the mesh.

The Lagrangian scheme [Ramaswamy et al., 1986; Thé et al., 1994 and Bellet and Chenot, 1993] had been used to model the moving boundary problem. The Lagrangian scheme is characterized by the mesh system which moves or deforms as the calculation proceeds. As a consequence of the large deformation of the free surface expected at the sloshing motion, numerical errors will be generated. Later on, this scheme had been used in the Smoothed Particle Hydrodynamics (SPH) method.

The SPH method was used to investigate the sloshing in tanks undergoing rolling motion; however it was found to be computationally expensive [Souto-Iglesias et al, 2004; Souto-Iglesias et al, 2006; Delorme et al, 2009; Fang et al, 2009]. This method relied on the idea of dividing the flow region into particles instead of meshes thus no boundary conditions are required at the free surface and consequently could capture phenomena such as wave breaking [Monaghan, 1988].

Another scheme had been used to develop numerical models is called "Eulerian scheme" [Torrey et al., 1986; Koh et al., 1994; Poo and Ashgriz, 1990; Rudman, 1997; Scardovelli and Zaleski, 1999; Tavakoli et al., 2006]. In this scheme, fixed grids had been used during the entire calculation. The evaluation of the convective flow fluxes required an averaging of the flow properties between the current calculating mesh and the neighboring grids. The averaging process could cause a smearing of the free surface discontinuity which is a serious drawback of the Eulerian scheme based models.

Yamamoto and Kawahara (1999) solved the Navier-Stockes equations by using arbitrary Lagrangian-Eulerian (ALE) formulation to predict the liquid motion. In this method, the re-meshing technique had been used to maintain the computational stability. The smoothing factor was introduced for stability, smoothing on the free surface, therefore finding a proper value for this factor was the major issue of this technique because it was very difficult to choose a unique constant for the entire computations.

Mapping technique is a new numerical model that was applied by Hamed and Floryan (1998) and Siddique et al. (2004) for the numerical modeling of moving boundary at the free surface. By this method, the irregular physical domain was transformed into a rectangular computational domain. Although this method could predict the sloshing motion of the liquid accurately and handle the free surface motion, it could not deal with surface discontinuities (e.g. wave breaking). A similar technique had also been employed by Frandsen and Borthwick (2003) and Frandsen (2004) to investigate the liquid sloshing inside a 2-D tank which was moved both horizontally and vertically.

In summary, the contributions and the limitations of the main numerical models is presented in Table (2.1):

**Table 2.1: The Contributions and the Limitations of the Main Numerical Models**

| Model | Contributions | Limitations |
|---|---|---|
| Potential flow theory | ➢ Considers incompressible, inviscid and irrotational flow. | Cannot investigate the free surface discontinuities. |
| Shallow-water wave theory | ➢ Solves nonlinear Navier Stokes eqns under the assumption of relatively low wave height compared to the mean depth of liquid layer. | Cannot handle high depth of water. |
| Lagrangian scheme | ➢ Solves moving-boundary problems. | Cannot handle large deformation of the free surface. |
| Eulerian scheme | ➢ Solves moving-boundary problems. | The averaging process could cause a smearing of the free surface discontinuity. |
| Mapping techniques | ➢ Solves the sloshing, nonlinear, moving-boundary problems.<br>➢ Can handle the free surface deformations. | Cannot deal with surface discontinuities. |
| Fully-nonlinear Navier Stokes Eqns with VOF Method | ➢ Involves all the Mapping techniques features.<br>➢ Can deal with surface discontinuities<br>➢ Less computational cost | Does not account for the all dynamic stresses on the free surface. Assume p=0 at the free surface, when TLD not covered. |

## 2.3 The Damping Effect of TLDs in tall buildings

As stated earlier, the induced vibration in high-rise buildings is caused primarily due to wind. Hence, an optimum TLD design of a tall building is required for comfort and serviceability. Accordingly, a multitude of theoretical and experimental studies have been done to investigate the TLD design performance characteristics.

TLDs had been used in a high-rise hotel, "Shin Yokohama Prince (SYP) Hotel" in Yokohama (see Figure 2.1). Wakahara et al. (1992) studied the effect of various design parameters on the TLD performance.

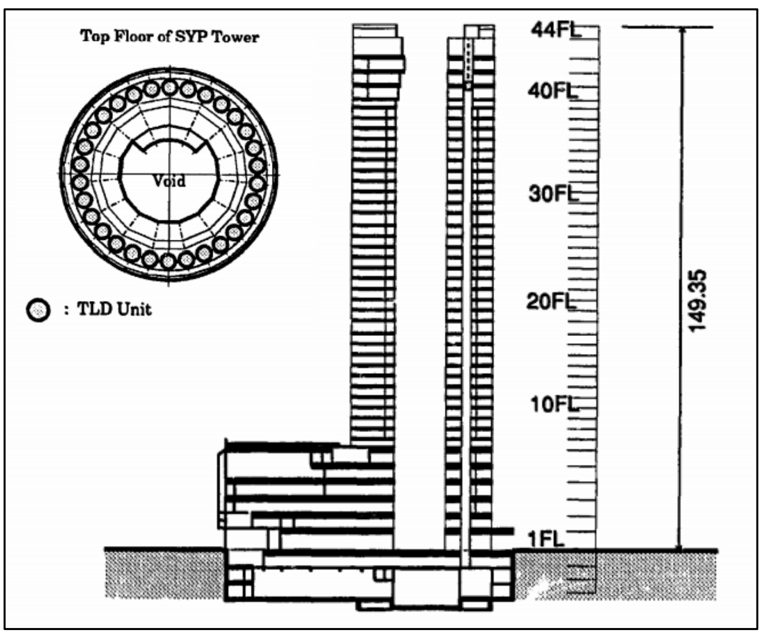


**Figure 2.1: A schematic of the SYP Hotel and Tower [Wakahara et al., 1992]**

Three main dimensionless parameters were considered: (1) the ratio of the liquid mass in the TLD to the structure mass (the mass ratio), (2) the ratio of the TLD natural frequency to the structure natural frequency (the frequency ratio), and (3) the damping constant of the liquid motion inside the TLD. Thirty (30) units of TLDs were installed on the top floor of the SYP hotel. Each of these units has nine (9) circular containers as TLDS. Each TLD has a diameter of 2 m and a total height of 2 m. They used a mass ratio of 1% and a damping constant of 5%. As a result, the TLD proved to effectively reduce the wind-induced response by 50% at an average wind speed of 20 to 30 m/s.

## 2.4 Research Scope and Objectives

As indicated before, many numerical models have been developed to investigate the sloshing motion inside TLDs. However, there has not been a study that incorporated a numerical model that can be used to assess the effect of wave breaking on the damping performance of TLDs coupled with structures. Therefore, the current study is numerical in nature, and uses an algorithm that has been developed at the Thermal processing Laboratory, Oda (2012), to study the effect of wave breaking on the performance of a TLD coupled with a structure. The following are the main objectives of the current study:

1- To assess the TLD damping performance under different operating conditions that could lead to wave breaking. The TLD operating conditions are represented by the TLD-Structure frequency ratio ($f_{TLD}/f_s$), the external excitation amplitude ratio (A/L) and the external excitation frequency ratio ($f_{TLD}/f_e$).

2- To develop an empirical correlation that can be used as a design tool to determine the optimum TLD designs under various operating conditions.

## 2.5 Organization of Thesis

Chapter three provides a brief description of the current numerical model, including the fluid and structure algorithms and the way they are coupled. Chapter four presents the details of the computational mesh, the mesh independent tests, and the validation of the numerical model. Chapter five presents the effect of the external excitation amplitude-TLD length ratio (A/L), External excitation frequency ratio ($f_{TLD}/f_e$) and TLD-Structure frequency ratio ($f_{TLD}/f_s$) on the TLD damping. The summary, conclusions and recommendations for future work are included in chapter 6.

# 3 Chapter 3: Mathematical Formulation and Numerical Model

The numerical model used is the one developed by Oda (2012) which solves the two-dimensional, incompressible, free surface, fluid flow inside a rectangular TLD. The model is capable of investigating the TLD-structure interaction. The model considers a TLD coupled with a single degree of freedom (SDOF) structure exposed to an external excitation force, as shown in Figure 3.1. The excitation force considered in this study is harmonic and unidirectional.

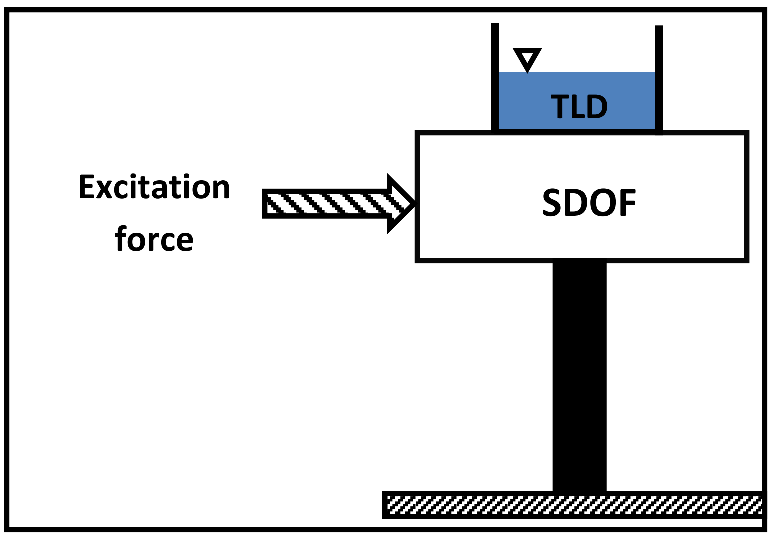


**Figure 3.1: Schematic of TLD-Structure coupling**

The TLD is considered as a rigid rectangular tank of Length, L, Height, H, Width W and initial liquid height h, as shown in Figure 3.2.

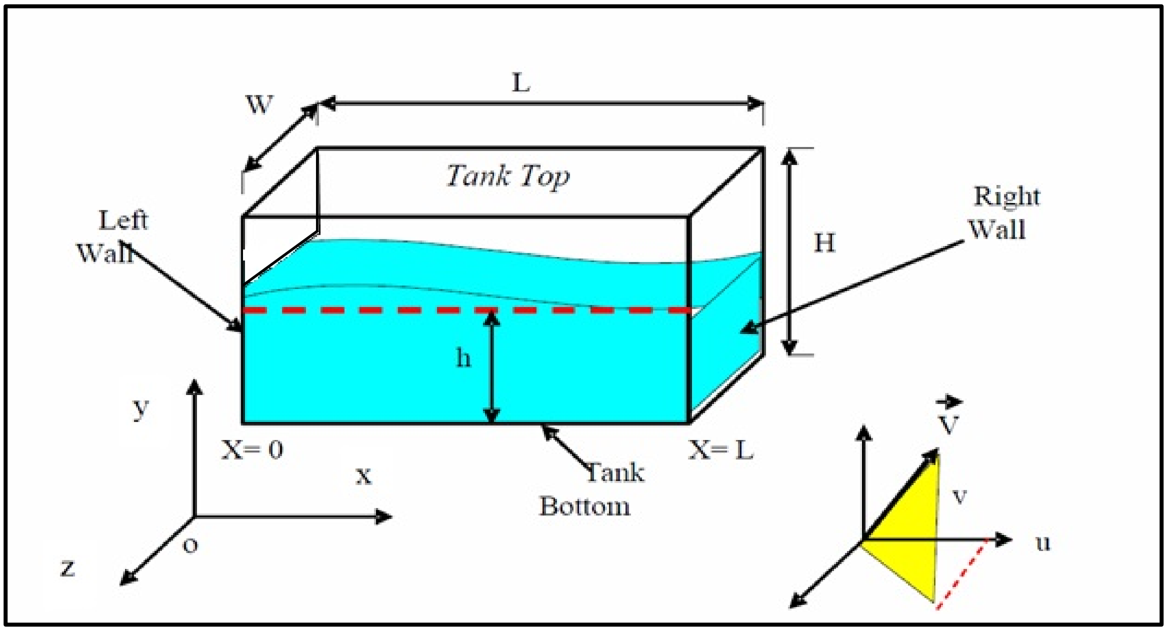


**Figure 3.2: Model Problem, the Cartesian coordinate system, and the Fluid Flow Velocity Components [Oda, 2012]**

### 3.1 The Governing Equations

Generally, there are two approaches to model free surface flows where there is an interface between two phases (gas and liquid), the one-phase and two-phase approaches. The current study adopts the one-phase approach, where the momentum equations are solved in for the liquid phase (water), while the gas phase (air) effect is considered through the free surface conditions. In the two-phase approach, the governing equations are solved in both phases (liquid and gas) by solving the variable density Navier–Stokes Equations (NSE).

The two-dimensional, incompressible, free surface, fluid flow problem has been modeled by using an Eulerian frame of reference using the Cartesian coordinates.

The governing equations of the incompressible, Newtonian, laminar flow in the Cartesian coordinate system are as follows:

- **<u>The Continuity Equation</u>**

$$\frac{\partial u}{\partial x} + \frac{\partial v}{\partial y} = 0 \qquad (3.1)$$

- **<u>The x-momentum equation</u>**

$$\frac{\partial u}{\partial t} + u\,\frac{\partial u}{\partial x} + v\,\frac{\partial u}{\partial y} = -\frac{1}{\rho}\frac{\partial p}{\partial x} + g_x + \frac{1}{\rho}\frac{\partial \tau_{xx}}{\partial x} + \frac{1}{\rho}\frac{\partial \tau_{xy}}{\partial x} \qquad (3.2)$$

- **<u>The y-momentum equation</u>**

$$\frac{\partial v}{\partial t} + u\,\frac{\partial v}{\partial x} + v\,\frac{\partial u}{\partial y} = -\frac{1}{\rho}\frac{\partial p}{\partial y} + g_y + \frac{1}{\rho}\frac{\partial \tau_{yy}}{\partial y} + \frac{1}{\rho}\frac{\partial \tau_{xy}}{\partial y} \qquad (3.3)$$

### 3.2 The Boundary Conditions

The no-slip and no-penetrating boundary conditions are applied on the TLD walls (left and right hand side wall and the bottom). The pressure at the left and the right TLD walls can be written as [Oda, 2012]:

$$p = \alpha * p * e^{\left(\frac{-y}{h}\right)} * sin(\omega\, t) \qquad (3.4)$$

Where, $\alpha * p$ is a parameter defined as the maximum pressure amplitude during the TLD excitation period. This equation has been developed based on the experimental work carried out by [Panigrahy et al, 2009] to determine the pressure distribution on the wall in the direction of the external harmonic excitation. Their findings indicated that the pressure on these walls changes in the same manner as the external excitation. However, the pressure at the bottom of the tank is set equal to the hydrostatic pressure of the liquid and it is calculated using the nominal (initial) liquid height.

At the free surface, the continuity of the velocity vector and stress components must be satisfied. For a two-dimensional flow, the stress boundary conditions are applied in the normal and the tangential directions. The stress boundary condition in the normal direction in this case is given by equation (3.5).

$$p_s - \sigma k = 2\mu n_k \frac{\partial u_k}{\partial n} \tag{3.5}$$

The stress boundary condition in the tangential direction is given by:

$$\mu\left(t_i \frac{\partial u_i}{\partial n} + n_k \frac{\partial u_k}{\partial s}\right) = \frac{\partial \sigma}{\partial s} \tag{3.6}$$

Where, σ is the liquid surface tension, $\frac{\partial}{\partial s} = \hat{t}.\nabla$ is the surface derivative and $\frac{\partial}{\partial n} = \hat{n}.\nabla$ is the normal derivative. Since the free surface is considered as a very thin layer, the viscous effects are neglected and the surface tension coefficient is assumed constant, subsequently; equation (3.5) can be written as:

$$p_s = \sigma k \tag{3.7}$$

### 3.3 Treatment of the Free Surface

The free surface is reconstructed using the Volume of Fluid Method [Hirt and Nichols, 1981; Lin, 2007]. The time evolution equation of the liquid free surface is calculated using the following equation:

$$\frac{\partial F}{\partial t} + u\frac{\partial F}{\partial x} + v\frac{\partial F}{\partial y} = 0 \qquad (3.8)$$

Where, F is the local volume fraction of the liquid phase. The F function is used to determine which cells contain a boundary and where the liquid is located in the cells. Therefore, F is equal to 1 when the cells are fully occupied with liquid phase and F is equal to 0 when the cells are occupied with the gas phase. F lies between zero and unity ($0 < F < 1$), if the cells contain the interface bounding the liquid and gas phases. Figure 3.3 shows a numerical example of F values in mesh cells in the liquid region, in the gas region, and along the free surface interface.

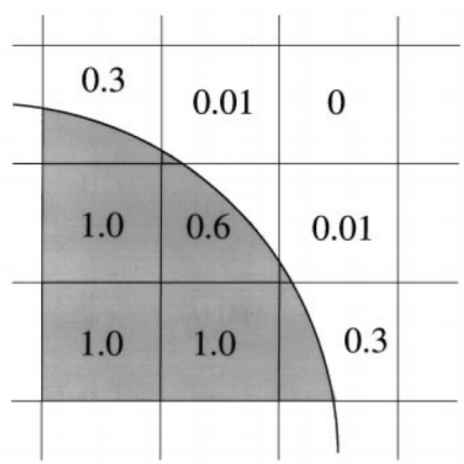


**Figure 3.3: Volume fraction values around a free surface interface [Bogdan A., 2010]**

The Donor-Acceptor technique has been used to determine the fraction area (the ratio between liquid to the total volume of the cell) of fluid flow. This technique is based on describing a surface orientation and then moving the surface with the velocity normal to that orientation. In the donor-acceptor technique, the surface cell is assumed to be either horizontal or vertical. The decision regarding the orientation is made based on studying the neighboring cells [Poo and Ashgriz, 1991]. By using this technique, the cells at the interface are identified; one cell as a donor which delivers the flow and the neighbor cell as an acceptor cell, which receives the flow. Accordingly, the subscript *D* denotes the donor cell, *A* denotes the acceptor cell and *AD* denotes either acceptor or donor, depending on the orientation of the interface relative to the direction of flow. The amount of liquid leaving the donor cell is exactly equal to the amount of liquid entering the acceptor through each computational face. Figure 3.4 shows the interface reconstruction using VOF method.

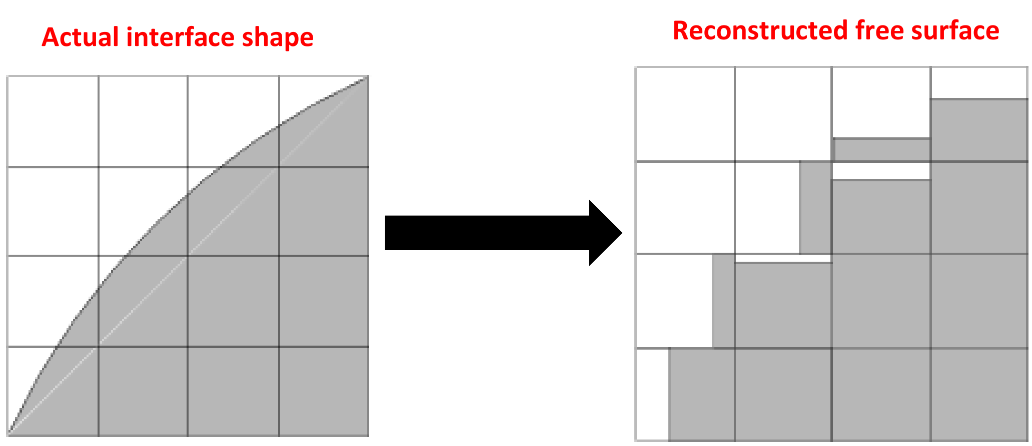


**Figure 3.4: Free surface reconstruction**
**[http://hmf.enseeiht.fr/travaux/CD0809/bei/beiep/9/html/vof/vof.html]**

The velocity and the pressure fields are calculated first by using an assumed liquid volume fraction ($F$), after that the value of $F$ is updated, and the process is iteratively repeated until the calculated values remain constant. The new $F$- field is calculated by solving equation (3.8). The conservative form of the $F$- field is determined by combining equation (3.8) with the continuity equation (3.1), as demonstrated by [Zang et al., 2000]:

$$\frac{\partial F}{\partial t} + \frac{\partial (F\, u)}{\partial x} + \frac{\partial (F\, v)}{\partial y} = 0 \tag{3.9}$$

As far as the free surface is concerned as per the occurrence of wave breaking, the Continuum Surface Force (CSF) model has been used in the current numerical work at the interface, [Brackbill, 1992]. The two fluids are characterized via a function, c ($\vec{x}$) as follows:

c ($\vec{x}$) = $c_1$ for liquid,

c ($\vec{x}$) = $c_2$ for air,

c ($\vec{\boldsymbol{x}}$) = $\langle \boldsymbol{c} \rangle$ = ($c_1$+ $c_2$) for the interface. (3.1)

The CSF model considers the replacement of the discontinuous characteristic function c ($\vec{x}$) by a smooth variation of fluid color $\tilde{c}$ ($\vec{x}$) from $c_1$ to $c_2$ over a distance of O(h*), where h* is the transition layer thickness and comparable to the resolution afforded by the calculation mesh size. Moreover, the volume force $\vec{F}_{SV}$ and a delta function have been used to reformulate the surface tension instead of the direct evaluation of the surface pressure using the Laplace's equation (3.7) [Lepelletier and Raichlen, 1988]. This equation can be written as:

$$lim_{h\to 0} \int_{\Delta V} \vec{F}_{SV} (\vec{x}) d^3x = \int_{\Delta S} \vec{F}_{Sa} (\vec{x}_S) dS \tag{3.11}$$

Where,

$$\vec{F}_{Sa} (\vec{x}_S) = F_S^{(n)} \hat{\mathrm{n}} + F_S^{(t)} \hat{\mathrm{t}} \tag{3.12}$$

$\vec{F}_{Sa} (\vec{x}_S)$ represents the surface force, while $\mathrm{F}_\mathrm{S}^{(\mathrm{n})}$ and $\mathrm{F}_\mathrm{S}^{(\mathrm{t})}$ are the surface force components along the unit normal ($\hat{\mathrm{n}}$) and the unit tangent ($\hat{\mathrm{t}}$), respectively. $\vec{x}_S$ is a point on the interfacial area $\Delta S$. As mentioned earlier, the viscous stresses at the free surface have been neglected and the surface tension coefficient $\sigma$ has been assumed to be constant. Therefore, the surface force around the interfacial area $\vec{F}_{Sa}$ will be equal to the surface force along the unit normal $F_S^{(n)}$, which leads to [Oda,2012]:

$$\vec{F}_{Sa}(\vec{x}_S) = \mathrm{F}_\mathrm{S}^{(\mathrm{n})}(\vec{x}_S) = \sigma k \, (\vec{x}_S) \, \hat{\mathrm{n}} \, (\vec{x}_S) \tag{3.13}$$

Finally, the surface tension force $F_S^{(n)}(\vec{x}_S)$ is added to the body force in the momentum equation.

### 3.4 Numerical Implementation

The momentum equation is solved using the Two-Step Projection Method. The time discretization form of the momentum equation for incompressible fluid flow is:

$$\frac{\vec{V}^{n+1} - \vec{V}^{n}}{\delta t} = -\nabla.(\vec{V}\,\vec{V})^{n} - \frac{1}{\rho^{n}}\,\nabla\,\rho^{n+1} + \frac{1}{\rho^{n}}\,\nabla.\tau^{n} + \vec{g}^{n} + \frac{1}{\rho^{n}}\,\vec{F}_{b}^{n} \qquad (3.14)$$

As the pressure gradient is the key in solving the discretized momentum equation, the pressure term was the implicit term in equation (3.14), while the other terms as the advection, body force, and viscous stresses were evaluated from the previous time step, denoted by the superscript (n). A two-step projection method has been used to split the momentum equation (3.14) into:

$$\frac{\tilde{V} - \vec{V}^{n}}{\delta t} = -\nabla.(\vec{V}\,\vec{V})^{n} + \frac{1}{\rho^{n}}\,\nabla.\tau^{n} + \vec{g}^{n} + \frac{1}{\rho^{n}}\,\vec{F}_{b}^{n} \qquad (3.15)$$

And,

$$\frac{\vec{V}^{n+1} - \tilde{V}}{\delta t} = -\frac{1}{\rho^{n}}\,\nabla\,\rho^{n+1} \qquad (3.16)$$

The legacy of velocity $(\tilde{V})$ field at the previous time step, according to the balance between the gravitational force, advection term, and the body forces, equation (3.15), is evaluated. The velocity field is corrected by using the pressure gradient term at the new time step to determine the new velocity field at the new time step, $(\vec{V}^{n+1})$, equation (3.16).

The continuity equation applied for the new time step denoted by the superscript (n+1) and expressed as:

$$\nabla . V^{n+1} = 0 \tag{3.17}$$

To evaluate pressure gradient, equations (3.16) and (3.17) were combined through the Poisson's equation, as follows:

$$\nabla . \left( \frac{1}{\rho^{n}} \nabla \rho^{n+1} \right) = \frac{\nabla . \tilde{V}}{\delta t} \tag{3.18}$$

One of the important features of the Pressure Poisson Equation (PPE) given by (3.18) is that the pressure gradient adapted by other forces affect the fluid element as the gravitational, body forces, the inertia forces, and the viscous stresses via the acceleration term $(\frac{\nabla . \tilde{V}}{\delta t})$ will be the corner stone to evaluate the new velocity field at the new time step (n+1), $V^{n+1}$.

### 3.5 Equation of Structure Motion

Studying the TLD-structure interaction is essential for investigating the damping performance and effectiveness of the TLD. The liquid sloshing motion inside the TLD produces a sloshing force ($F_{TLD}$), which is desirably anti-phase with the external excitation force ($F_e$), and thus it produces a damping effect that reduces the swaying motion of the structure. In the current study, the TLD was coupled with a SDOF structure as shown in Figure 3.5. The SDOF can be defined in terms of its mass, $\mathbf{M_S}$, stiffness,

$\mathbf{K_S}$, and damping coefficient, $\mathbf{C_S}$. The equation of motion of the coupled system can be expressed as:

$$M_S \ddot{X}_S + C_S \dot{X}_S + K_S X_S = F_e + F_{TLD} \tag{3.19}$$

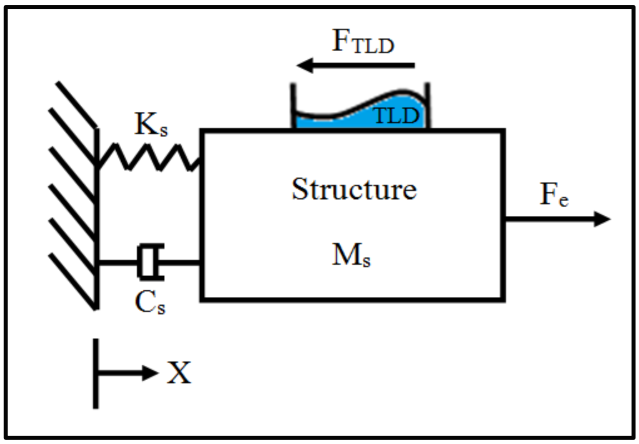


**Figure 3.5: Schematic of the TLD - structure (SDOF) interaction model**

The damping force ($F_{TLD}$) can be calculated from the rate of change of the liquid momentum inside the TLD using the following equation:

$$F_{TLD} = \frac{1}{\Delta t}\left(P(t) - P(t + \Delta t)\right) \tag{3.20}$$

Where, P*(t)* is the total momentum of the liquid inside the TLD.

Since structures in real applications could be exposed to random loads, the Duhamel integral method has been used to solve the equation of motion of the structure under all types of external excitations, whether random or harmonic.

The total displacement of the damped SDOF system is given by:

$$X_S(t) = e^{-\zeta\omega_n t}\left(X_0 \cos\omega_D t + \frac{u_0 + X_0 \xi\omega_n}{\omega} \sin\omega_D t\right) \qquad (3.21)$$

Where,

$$\omega_D = \omega_n \sqrt{1-\zeta^2} \qquad (3.22)$$

Where, $X_S(t)$ is the response for the damped system in terms of the Duhamel's integral, and $\omega_D$ is the damped frequency of the structure. The particular solution of the structure equation of motion can be expressed as:

$$X_S(t) = \frac{1}{M_S \omega_D} \int_0^t F_t(\tau) e^{-\zeta\omega_n(t-\tau)} \sin\omega_D(t-\tau)\, d\tau \qquad (3.23)$$

Where, $F_t$ is the summation of the external excitation force and the TLD sloshing force.

Detailed computations of the Duhamel integrals can be found in Paz M, 1997 and Marivani and Hamed, 2009.

### 3.6 The Flow Chart of the Current Numerical Model

The flow chart of the present numerical model is shown in Figure 3.6.

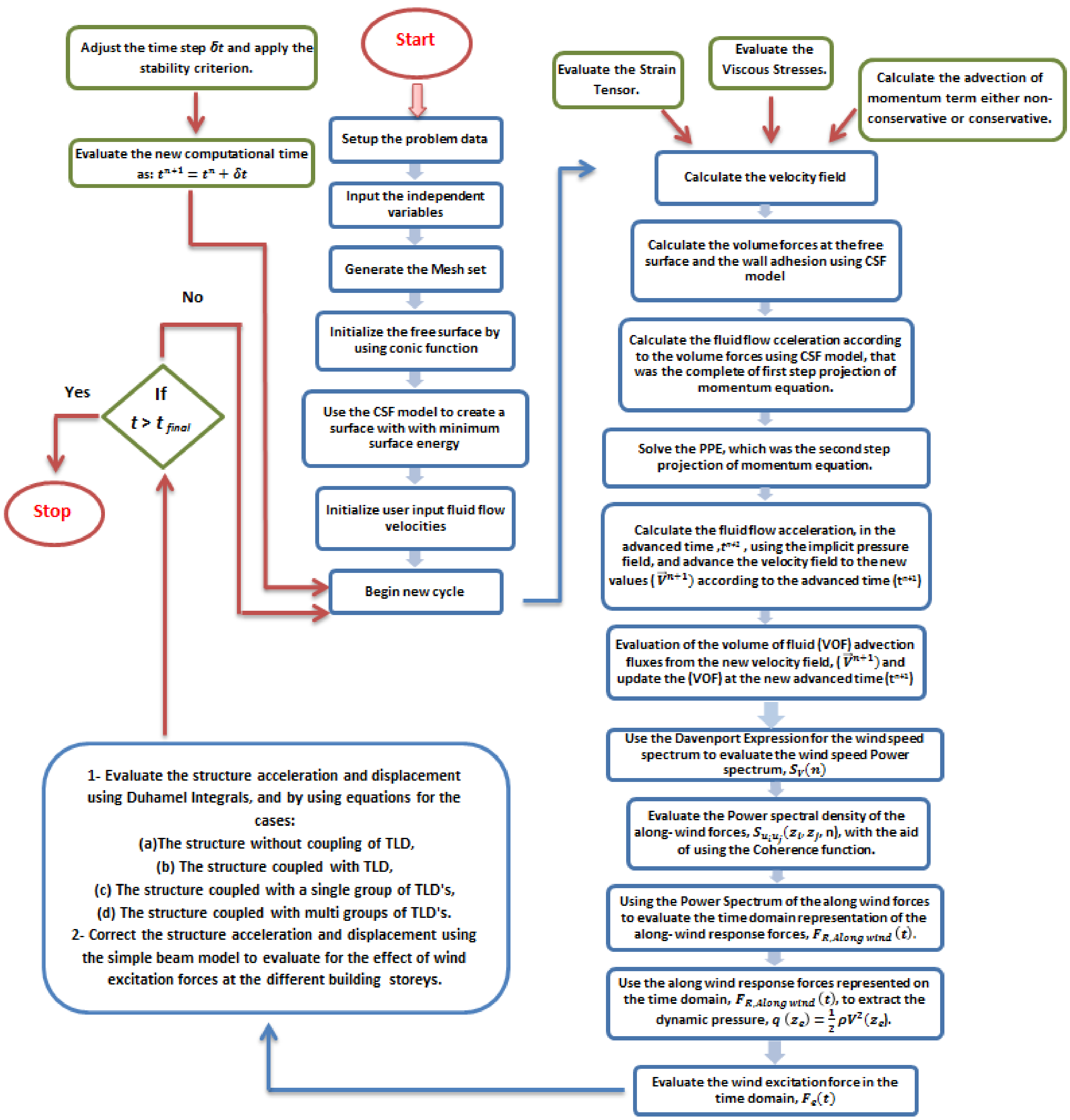


**Figure 3.6: Flow Chart of Two-dimensional Numerical Model**

# 4 Chapter 4: Numerical Model Validation

## 4.1 Design of the Computational Grid and selection of the computational time step

The computational grid used in this study is a non-uniform grid. Non-uniform grids are more suitable than uniform grids in dealing with boundary layer problems and free-surface flows. The current numerical model divides the main domain into 5 subdomains in x-axis and y-axis as shown in Figure 4.1, then each subdomain is divided into two regions around a selected point called the convergence point and it is chosen nearby the region where the dependent variables are expected to vary drastically [Murakami,1997].

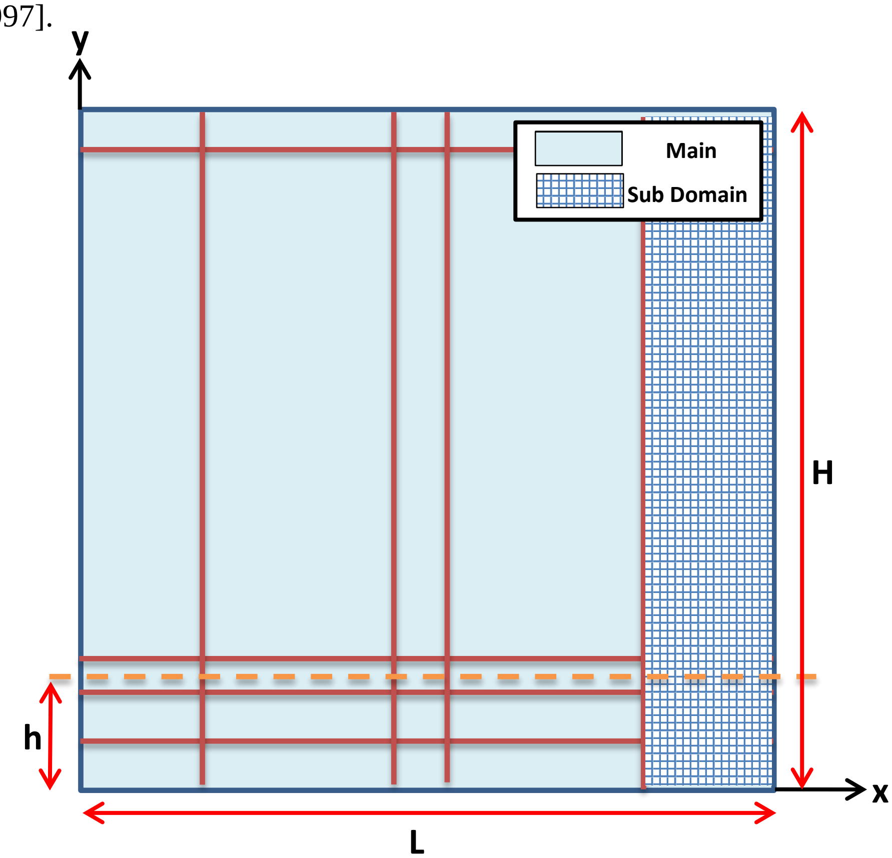


**Figure 4.1: Schematic of the grid**

A quadratic function ($x = \varepsilon^2$) was used to stretch the uniform grid spacing ($\Delta$x) to the non-uniform grid spacing ($\Delta\varepsilon^2$) as shown in Figure 4.2, where it is the actual mesh generation for TLD with length (L) =1.0 m and 104 cells in x-direction, 60 cells in y-direction.

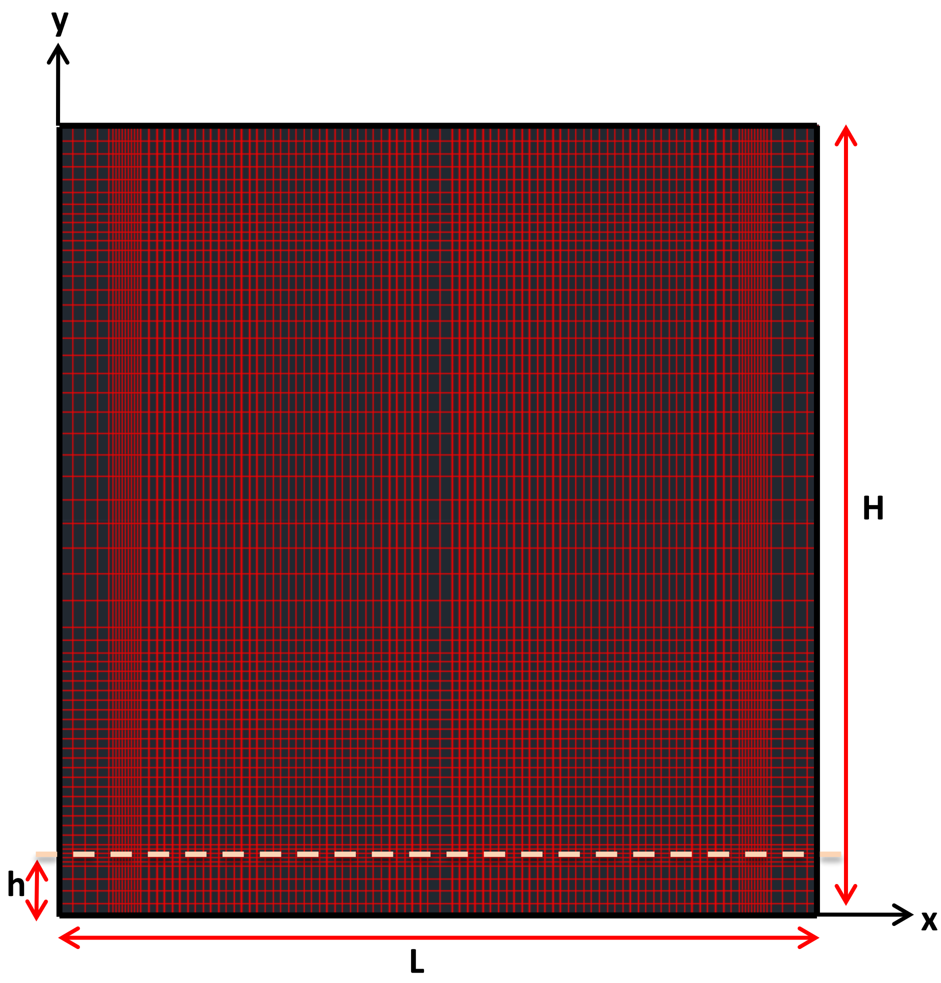


**Figure 4.2: The non-uniform computational grid used for the case of h/L = 0.35**

The momentum transport equation and the free surface time-evolution equation used in the VOF method are explicit equations in time. Therefore, a set of stability conditions had to be satisfied. The Courant time limit was used to determine the time step in x- and y- directions, $(\delta t_{cx}, \delta t_{cy})$.

The courant time step limit $(\delta t_c)$ should be taken as the minimum of $\delta t_{cx} and\ \delta t_{cy}$; i.e., the computation time step selected according to equation (4.1).

$$\delta t \quad \leq \left\{\delta t_c = \min(\delta t_{cx}, \delta t_{cy})\right\},$$

And

$$\delta t_{cx} = C^* \left\{\frac{\delta x}{|u|}\right\}_{min}, \delta t_{cy} = C^* \left\{\frac{\delta y}{|v|}\right\}_{min} \tag{4.1}$$

The value of the Courant multiplier ($C^*$) in the current numerical work is **0.3** [Floryan and Rasmussen, 1989; Murakami, 1993].

Another important stability criterion was considered due to the diffusion process. In order to avoid negative diffusion, the computational time step must also satisfy the following condition [Murakami, 1993]:

$$\delta t \leq \min\left(\frac{\rho \Delta x^2}{6\mu}, \frac{\rho \Delta y^2}{6\mu}\right) \tag{4.2}$$

The computational time step used in the current study is $6.62 * 10^{-4}$ sec.

## 4.2 Mesh Independence Test

Computational results should not depend on the size of the computational grid. Therefore, a grid independence test was carried out. Three mesh sizes, 104 x 60, 208 x 120, and 400 x 200 were selected and the maximum deviation in a calculated parameter was determined.

Table (4.1) shows the maximum difference in the calculated acceleration of structure using the different mesh sizes relative to the 104 x 60 mesh. Based on these results, the 104 x 60 mesh was considered satisfactory, and hence it was used throughout the current study.

**Table 4.1: Results of the mesh independence test**

| Mesh size | Maximum deviation |
|---|---|
| 104 x 60 | Selected mesh |
| 208 x 120 | 0.75 % |
| 400 x 200 | 4.37 % |

Figure 4.3 shows the variation in the TLD acceleration coupled with the SDOF calculated using the three meshes listed in Table (4.1). It can be observed that the variations between the different mesh sizes are insignificant. Another test was carried out to check the effect of minimum grid sizes.

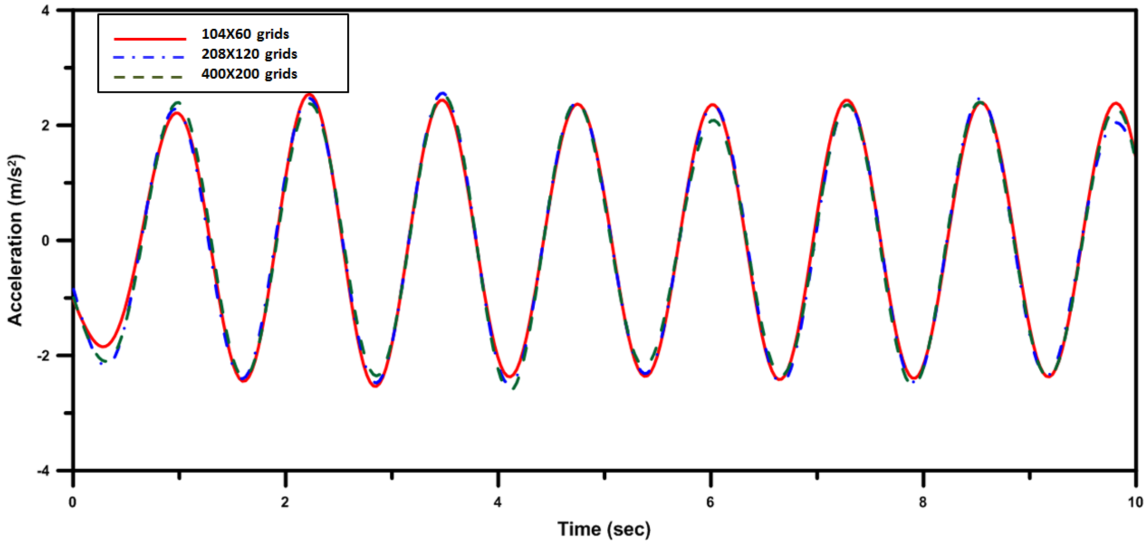


**Figure 4.3: TLD acceleration time history determined using the three grids listed on Table 4.2.**

Table (4.2) shows the maximum difference for the acceleration at two different minimum grid sizes relative to 16 mm.

**Table 4.2: Grid Size Analysis**

| Grid size | Maximum deviation |
|---|---|
| 16 X 16 | Selected mesh |
| 8 X 8 | 0.1 % |
| 4 X4 | 2.93 % |

Figure 4.4 shows the variation of the acceleration of the TLD coupled with the SDOF as determined using the three different minimum cell sizes listed in Table (4.3). It can be noticed that the variations between the different minimum cell sizes are acceptable.

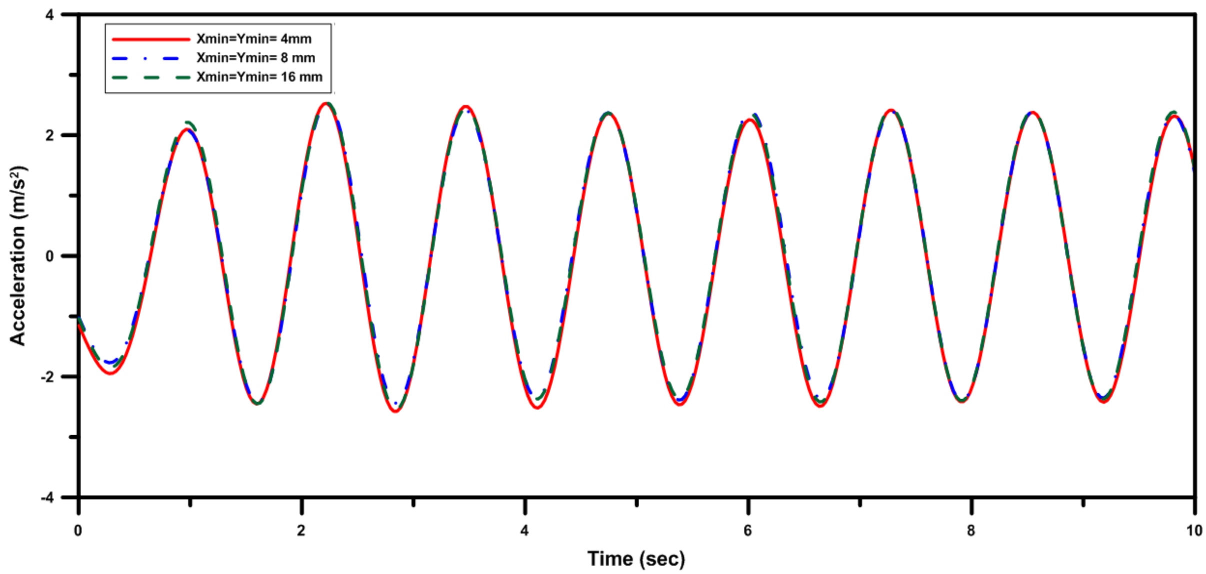


**Figure 4.4: Acceleration time history for different cell size**

## 4.3 Model Validation

The validation of the present numerical model has been carried out by comparing the numerically predicted free surface with the one measured experimentally. These validations have been reported by Oda (2012,2013 and 2014)

### *4.3.1 Model Validation - Case study (1)*

The first validation has been carried out by comparing numerical results obtained using the current model with the experimental data reported by Colagrossi et al (2004). The carried out an experimental study of a rectangular TLD with length (L) = 1.0 m, height (H) = 1.0 m, width (w) = 0.1 m. The tank had an initial depth of water (h) of 0.35 m. The TLD was exposed to an external, harmonic (sinusoidal), unidirectional excitation of amplitude (A) = 0.05 m, linear sloshing period ($T_1$) = 1.14 sec, and excitation frequency (*f*) = 0.792 Hz. Figure 4.5 shows a schematic of the TLD used in their study.

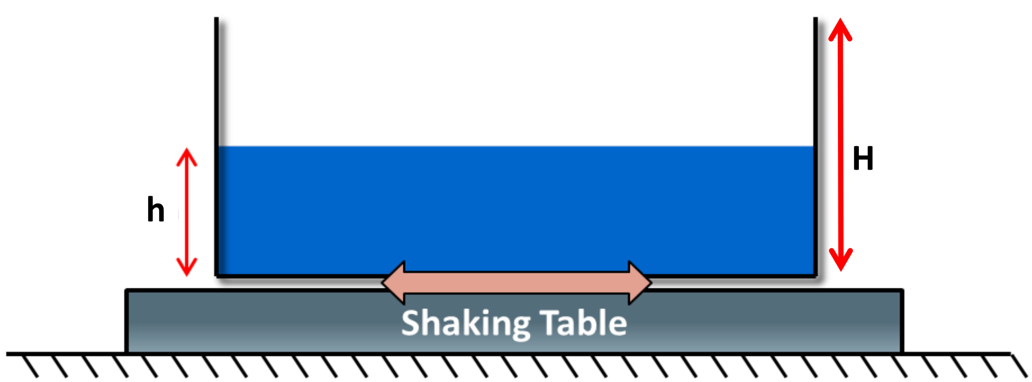


**Figure 4.5: Schematic of the TLD used in Colagrossi et al (2004).**

A comparison of the numerically predicted free surface and a snap shot of the free surface at time = 19.4 T= 24.48 sec is presented in Figure 4.6. T is the excitation period = 1.262 sec.

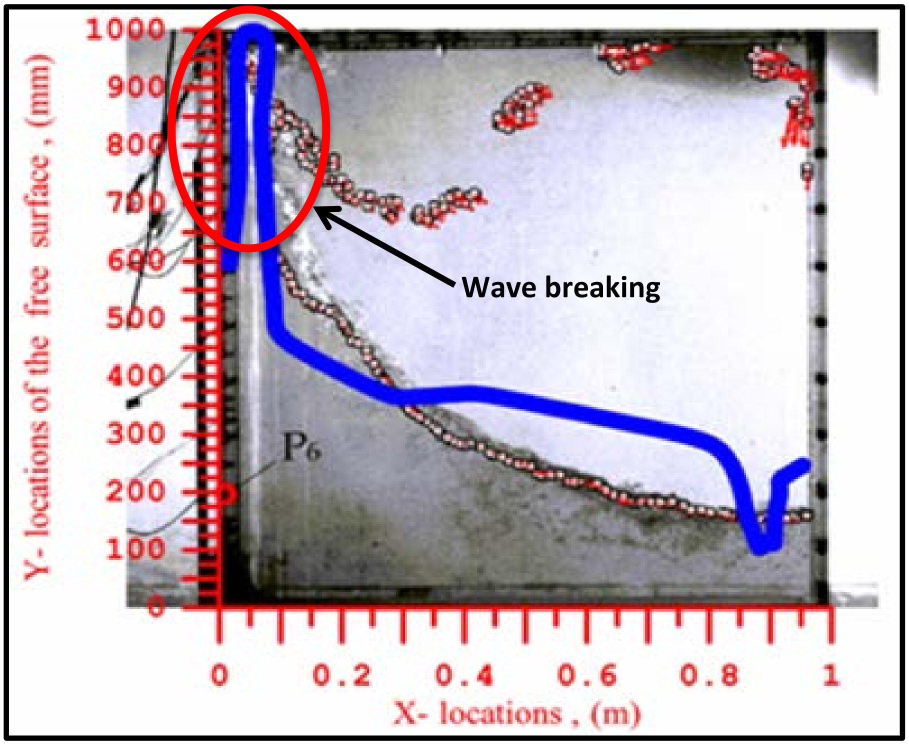


**Figure 4.6: Comparison of the numerically predicted free surface and the free surface recorded by Colagrossi et al (2004) t = 24.48 sec. Reprint from Oda 2012.**

Figure 4.6 confirms the capability of the current numerical in predicting the liquid free surface reasonably well, as well as its ability to capture the significant surface non-linearity (wave runner up) captured experimentally.

*4.3.2 Model Validation - Case study (2)*

The numerically predicted free surface was compared with experimental test results reported by Tait et al. (2005). In their experimental study, a TLD was subjected to a unidirectional, horizontal, harmonic (sinusoidal), external excitation. The TLD was attached to a 1:10 model of a structure building. The TLD was rectangular in shape with length (L) = 0.966 m, width = 0.36m and the initial water depth of water, (h), of 0.119 m. A schematic of their TLD is shown in Figure 4.7. The external excitation displacement imposed on the TLD is given in equation (4.3).

$$X_e = A\sin(\omega t + \varphi) \tag{4.3}$$

The amplitude A, the period T, and the phase angle φ were 25.9 mm, 1.681s and $4^0$, respectively. A wave probe was mounted to measure the free surface elevation at a distance x =0.0483 mm from the left hand side of the TLD wall.

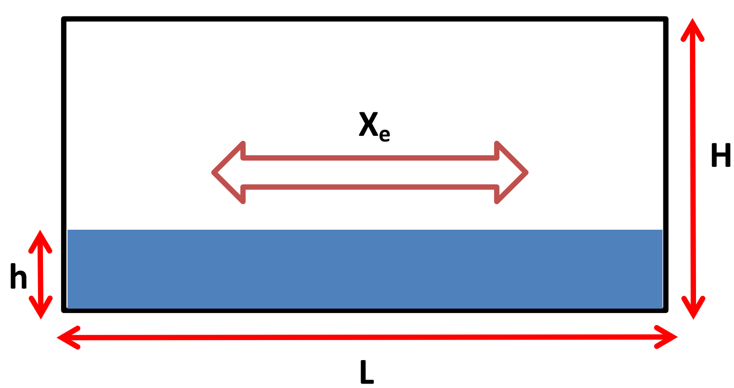


**Figure 4.7: TLD Tank used in experimental study carried by Tait et al. (2005).**

The direct comparison between the measure height of the free surface and the numerically predicted height for a period of 30 seconds is shown in Figure 4.8.

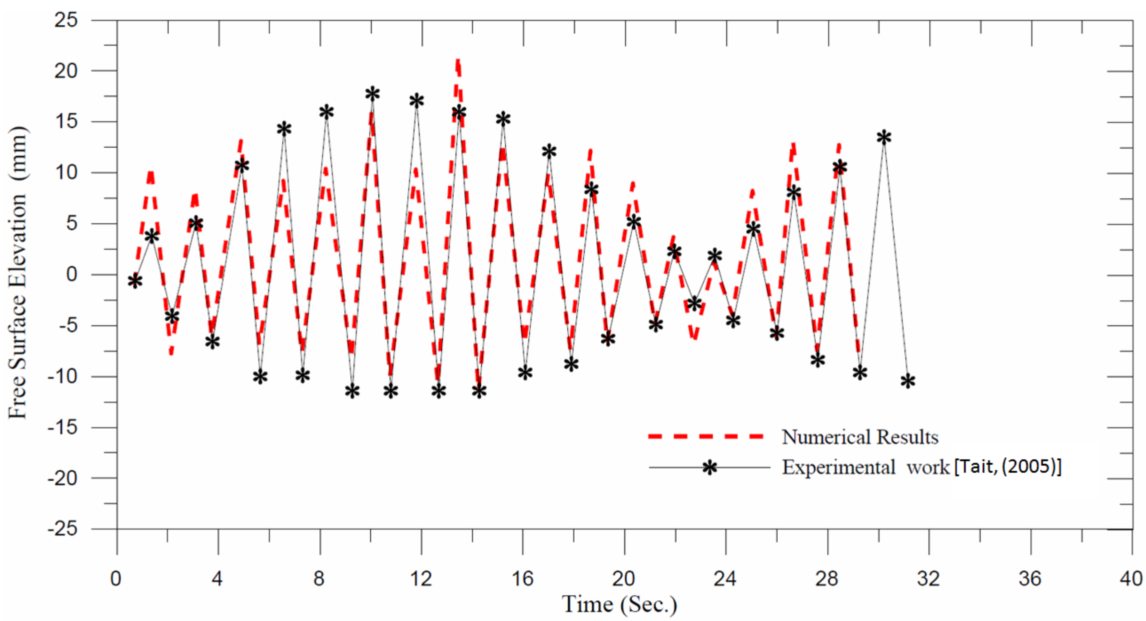


**Figure 4.8: Comparison between numerically predicted free surface elevations with experimental data reported in Tait et al. (2005). Reprint from Oda 2014.**

### *4.3.3 Model validation - Case study (3)*

Kim Y, 2001 investigated wave breaking and the impact of the wave on the tank cover inside partially filled TLDs (70% filled). A TLD was subjected to a sinusoidal excitation with an amplitude A = 0.038 m and a period T = 0.98 sec. The TLD was length (L) = 0.8 m and height = 0.54m. The liquid free surface hits the tank top and consequently imposes an impulse in the hydrodynamic pressure. Kim measured such impulses using pressure cells attached at the TLD cover. A comparison of the numerical results of the pressure impulses and the experimental results reported in Kim Y, 2001 are shown in Figure 4.9.

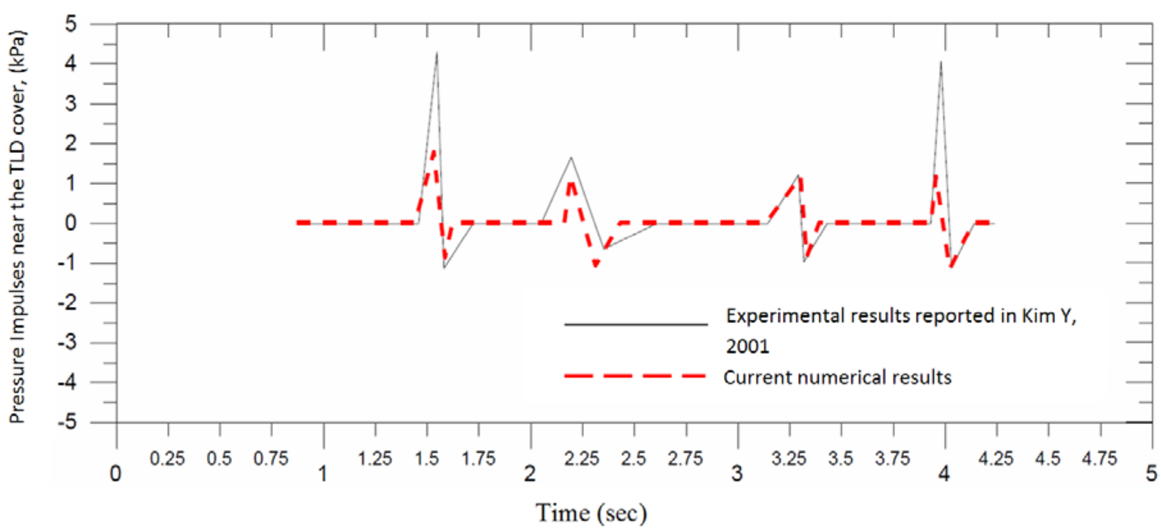


**Figure 4.9: Comparison between numerically predicted pressure impulses on the TLD cover caused by sloshing motion inside the TLD and experimental data reported by Kim Y, 2001.**

### *4.3.4 Model validation - Case study (4)*

Li et al., 2003 carried out an investigation of TLD damping effectiveness. They placed a number of TLDs on the 68th floor of a building at a height of 298 m above the ground level. They used a pair of accelerometers placed at the same level of the building to measure the structure acceleration, due to wind, in the x- and y- directions. The same case has been simulated using the current numerical model and the time history of the structure acceleration in the x-direction due to wind was predicted numerically and compared with experimental results reported in Li et al., 2003. A good agreement is shown in Figure 4.10.

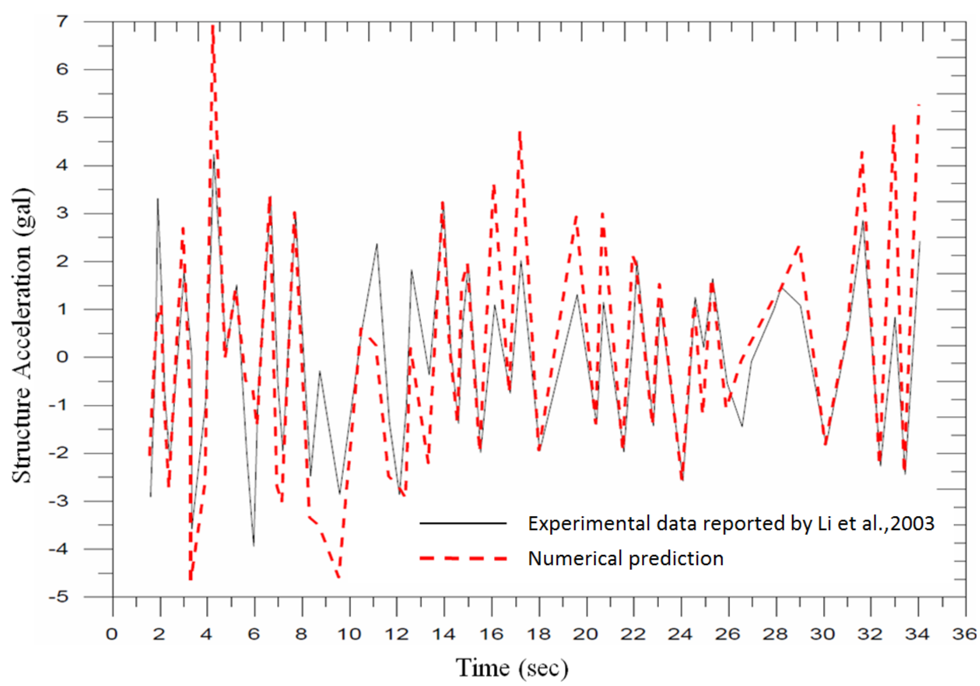


**Figure 4.10: The time history of a high-rise building acceleration determined using the current model and the acceleration time history measured experimentally by Li et al., 2003. Reprint from Oda 2013.**

The four validation cases discussed above confirm the capability of the current numerical model in predicting the sloshing motion of the liquid inside the TLD, including wave breaking and in predicting structure response due to external excitations.

# 5 Chapter 5: Numerical Results

Sun et al. (1992) reported that the optimum value of the liquid frequency is a value near the excitation frequency (resonance) that means tuning the TLD frequency to the natural frequency of the structure will provide significant amount of energy dissipation. For this reason, the selected cases were varied around the resonance.

## 5.1 Operating Parameters

As indicated before, one of the main objectives of this study is to use the present numerical model to investigate the damping performance of the TLD coupled with a SDOF structure. The geometrical and dynamic parameters that have been selected to study the TLD- Structure system are the following:-

1. The external excitation amplitude-TLD length ratio, A/L.
2. The TLD-external excitation frequency ratio, $f_{TLD}/f_e$.
3. The TLD-structure frequency ratio $f_{TLD}/f_s$.

Where, A is the maximum amplitude of the external harmonic excitation, L is the TLD length, measured in the direction of the external excitation, and $f_{TLD}$ is the water natural frequency, which can be calculated from the linear-wave theory using equation (5.1) (Lamb, 1932).

$$f_{TLD} = \frac{1}{2\pi}\sqrt{\frac{\pi g}{L}\tanh\left(\frac{\pi h}{L}\right)} \tag{5.1}$$

h in equation (5.1) is the initial liquid height in the TLD and $f_s$ is the structure natural

$$f_s = \frac{1}{2\pi} \sqrt{\frac{K_s}{m_s}} \tag{5.2}$$

frequency, which can be evaluated by using the following equation:

In Equation (5.2), $m_s$ and $K_s$ are the structure mass and stiffness, respectively. The structure considered in this study is a single degree of freedom (SDOF) with the properties listed in Table (5.1).

**Table 5.1: Properties of the SDOF structure considered in this study**

| $m_s$ (Kg) | $K_s$ (N/m) | $\zeta$ (%) |
|---|---|---|
| 1000 | 10,000 | 5.0 |

The dimensions of the TLD coupled with the SDOF structure are listed in Table (5.2).

**Table 5.2: Dimensions of the TLD considered in this study**

| L (m) | H (m) | W (m) |
|---|---|---|
| 1.0 | 1.0 | 0.1 |

The structure was subjected to a harmonic external excitation in the form,

$$X_e = A \sin (2\pi f_e\, t) \tag{5.3}$$

Where, A is the maximum amplitude of the external excitation.

The selected cases are classified into three main groups, according to the value of the TLD-structure frequency ratio, which was selected at 1.033, 1.093, and 1.153. These values are selected low structure natural frequencies, which corresponds to low structure stiffness, which overbears a wide range of building materials.

In each case, the excitation frequency was varied at three levels: (1) below resonance, (2) at resonance, and (3) above the resonance. Hence, the selected values of the TLD-excitation frequency ratio are 0.95, 0.98, 1.0, and 1.03. The excitation amplitude ratio was also varied in the range from 0.03 to 0.1.Details of all case considered for each of the three groups are listed in Tables (5.3, 5.4, and 5.6), for $f_{TLD}/f_s$ = 1.033, 1.093, and 1.153, respectively.

**Table 5.4: Group I, $f_{TLD}/f_s$=1.033**

| | h/L | $f_w/f_e$ | $f_e$ (Hz) | A/L |
|---|---|---|---|---|
| **Group I** $f_{TLD}/f_s$=1.033 | 0.115 | 0.95 | 0.547 | 0.03 |
| | 0.115 | 0.95 | 0.547 | 0.05 |
| | 0.115 | 0.95 | 0.547 | 0.07 |
| | 0.115 | 0.95 | 0.547 | 0.085 |
| | 0.115 | 0.95 | 0.547 | 0.1 |
| | | | | |
| | 0.115 | 0.98 | 0.531 | 0.05 |
| | 0.115 | 0.98 | 0.531 | 0.07 |
| | 0.115 | 0.98 | 0.531 | 0.085 |
| | 0.115 | 0.98 | 0.531 | 0.1 |
| | | | | |
| | 0.115 | 1 | 0.52 | 0.03 |
| | 0.115 | 1 | 0.52 | 0.05 |
| | 0.115 | 1 | 0.52 | 0.07 |
| | 0.115 | 1 | 0.52 | 0.085 |
| | 0.115 | 1 | 0.52 | 0.1 |
| | | | | |
| | 0.115 | 1.03 | 0.505 | 0.03 |
| | 0.115 | 1.03 | 0.505 | 0.05 |
| | 0.115 | 1.03 | 0.505 | 0.07 |
| | 0.115 | 1.03 | 0.505 | 0.085 |
| | 0.115 | 1.03 | 0.505 | 0.1 |

**Table 5.3: Group II, $f_{TLD}/f_s$=1.093**

| | h/L | $f_w/f_e$ | $f_e$ (Hz) | A/L |
|---|---|---|---|---|
| **Group II** $f_{TLD}/f_s$=1.093 | 0.13 | 0.95 | 0.579 | 0.03 |
| | 0.13 | 0.95 | 0.579 | 0.05 |
| | 0.13 | 0.95 | 0.579 | 0.07 |
| | 0.13 | 0.95 | 0.579 | 0.085 |
| | 0.13 | 0.95 | 0.579 | 0.1 |
| | 0.13 | 0.95 | 0.579 | 0.115 |
| | | | | |
| | 0.13 | 0.98 | 0.561 | 0.05 |
| | 0.13 | 0.98 | 0.561 | 0.07 |
| | 0.13 | 0.98 | 0.561 | 0.085 |
| | 0.13 | 0.98 | 0.561 | 0.1 |
| | 0.13 | 0.98 | 0.561 | 0.115 |
| | | | | |
| | 0.13 | 1 | 0.55 | 0.03 |
| | 0.13 | 1 | 0.55 | 0.05 |
| | 0.13 | 1 | 0.55 | 0.07 |
| | 0.13 | 1 | 0.55 | 0.085 |
| | 0.13 | 1 | 0.55 | 0.1 |
| | 0.13 | 1 | 0.55 | 0.115 |
| | | | | |
| | 0.13 | 1.03 | 0.534 | 0.03 |
| | 0.13 | 1.03 | 0.534 | 0.05 |
| | 0.13 | 1.03 | 0.534 | 0.07 |
| | 0.13 | 1.03 | 0.534 | 0.085 |
| | 0.13 | 1.03 | 0.534 | 0.1 |
| | 0.13 | 1.03 | 0.534 | 0.115 |

**Table 5.5: Group III, $f_{TLD}/f_s$=1.153**

| | h/L | $f_w/f_e$ | $f_e$ (Hz) | A/L |
|---|---|---|---|---|
| Group III $f_{TLD}/f_s$=1.153 | 0.147 | 0.95 | 0.611 | 0.05 |
| | 0.147 | 0.95 | 0.611 | 0.07 |
| | 0.147 | 0.95 | 0.611 | 0.085 |
| | 0.147 | 0.95 | 0.611 | 0.1 |
| | 0.147 | 0.95 | 0.611 | 0.115 |
| | | | | |
| | 0.147 | 0.98 | 0.592 | 0.05 |
| | 0.147 | 0.98 | 0.592 | 0.07 |
| | 0.147 | 0.98 | 0.592 | 0.085 |
| | 0.147 | 0.98 | 0.592 | 0.1 |
| | 0.147 | 0.98 | 0.592 | 0.115 |
| | | | | |
| | 0.147 | 1 | 0.58 | 0.05 |
| | 0.147 | 1 | 0.58 | 0.07 |
| | 0.147 | 1 | 0.58 | 0.085 |
| | 0.147 | 1 | 0.58 | 0.1 |
| | 0.147 | 1 | 0.58 | 0.115 |
| | | | | |
| | 0.147 | 1.03 | 0.505 | 0.05 |
| | 0.147 | 1.03 | 0.505 | 0.07 |
| | 0.147 | 1.03 | 0.505 | 0.085 |
| | 0.147 | 1.03 | 0.505 | 0.1 |
| | 0.147 | 1.03 | 0.505 | 0.115 |

## 5.2 TLD Energy Dissipation Capability

In order to assess the TLD damping capability, the amount of energy dissipated by the TLD must be calculated and normalized by the amount of energy imparted by the external excitation force. Consequently, the energy dissipation ratio (EDR) was defined and calculated. The EDR is defined as the ratio of the net energy imparted on the structure ($E_n$) with the TLD being used and the energy imparted by the external excitation force, $E_e$. The net energy imparted on the structure, with the TLD being used, $E_n$, equals to the difference between the energy imparted by the external excitation force, $E_e$, and the energy absorbed by the TLD, $E_{TLD}$. Therefore, the energy dissipation ratio, EDR, was calculated using equation (5.4).

$$EDR = \frac{E_e - E_{TLD}}{E_e} \tag{5.4}$$

Since the damping effectiveness of the TLD depends on the liquid sloshing motion, which is function of time, the value of the EDR is time-dependent. Hence, it was calculated as a function of time. The steady-state value of the EDR was used to assess the damping performance of the TLD. Steady-state was assumed to be reached when the instantaneous value of the EDR was within 1-2 % from its average value over the entire time considered in the simulation. Figure 5.2 shows the time history of the EDR obtained for, A/L = 0.085 and 0.1. In both cases, $f_{TLD}/f_s$=1.033 and $f_{TLD}/f_e$=1.0. In both cases, steady-state was reached after about 35 seconds.

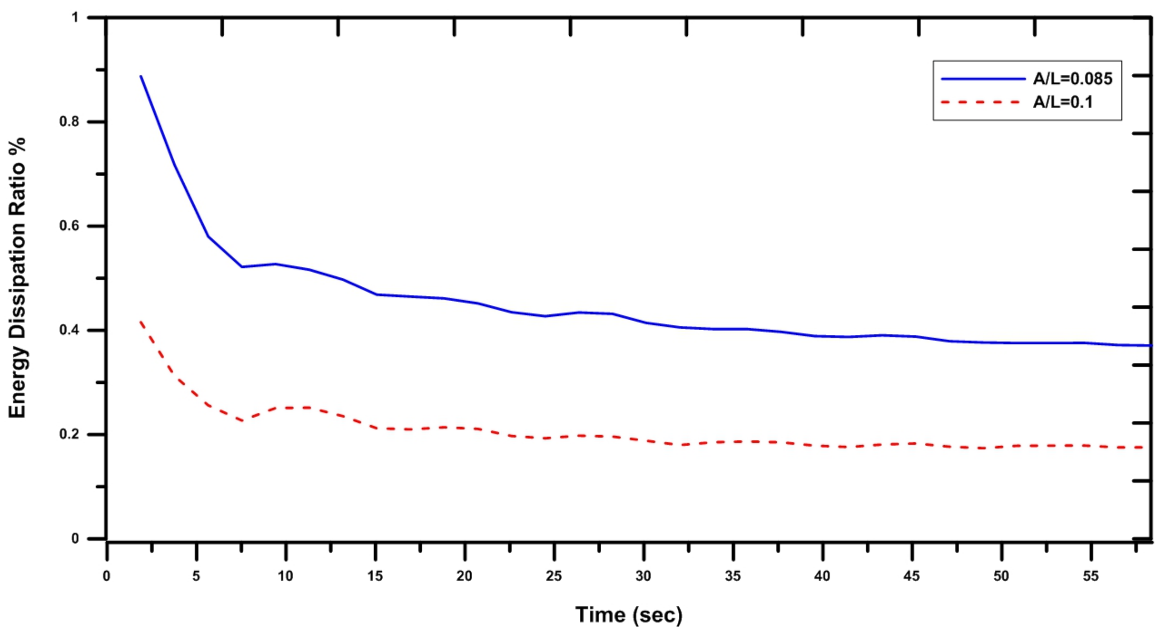


**Figure 5.1:Time history of the EDR calculated for the case of $f_{TLD}/f_s$=1.033, $f_{TLD}/f_e$=1.0, A/L = 0.085 and 0.1.**

### 5.3 The Energy Dissipation Factor

Because the calculated values of the EDR were sometime very small or very large, which made hard to compare, another parameter, called the Energy Dissipation Factor (EDF) has been proposed and used in the present study to quantify the TLD damping effect. The EDF is defined as the exponential of the EDR. This way the big difference between the various values of the EDT can be narrowed down. Thereby, the results can be classified into the following three categories: if EDF>1, then there is damping, if EDF=1, no damping (threshold of damping), and if EDF<1, there is negative damping or amplifying. The damping happens when the value of $E_{TLD}$ is less than $E_e$ this means the TLD absorbs part of the external excitation energy and in this case the sloshing force produced by the TLD is anti-phase with the external excitation force. If the value of $E_{TLD}$ is bigger than $E_e$ this means the sloshing force produced by the TLD is in-phase with the external excitation force, and consequently the TLD increased the external excitation seen by the building.

## 5.4 TLD-External Excitation Frequency Ratio ($f_{TLD}/f_e$) and Amplitude-TLD length Ratio (A/L) effects at Constant TLD-Structure Frequency Ratio ($f_{TLD}/f_s$)

The effects of the TLD-external excitation frequency ratio and the amplitude-TLD length ratio have been studied considering the three values of $f_{TLD}/f_s$ = 1.033, 1.093 and 1.153.

### *5.4.1 Group I, $f_{TLD}/f_s$=1.033*

Figure 5.2 shows the effect of the external excitation frequency ratio on TLD damping at different amplitude-TLD length ratios.

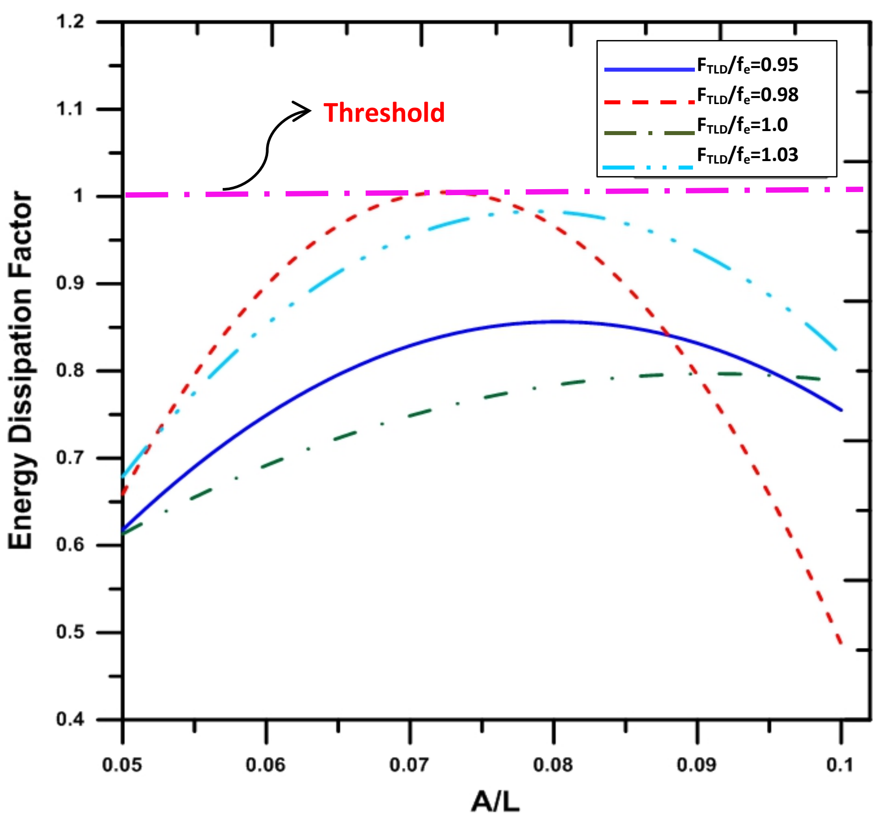


**Figure 5.2: Variation of energy dissipation factor as function of $f_{TLD}/f_e$ and A/L at $f_{TLD}/f_s$=1.033**

Results shown in Figure 5.2 indicate that in the case of $f_{TLD}$ /$f_s$ =1.033, the sloshing force produced by the TLD was in-phase with the external excitation force, and hence, no damping was produced by the TLD for all cases considered in this group. However, the threshold line which demarcates the boundary of the TLD damping range is tangent to case of fTLD/$f_e$ = 0.98 in the vicinity of the excitation amplitude ratio 0.07 to 0.075.

A contour [plot of the results shown in Figure 5.2 is shown in Figure 5.3 for the case of $f_{TLD}/f_s$ = 1.033. The light blue area in Figure 5.3 demarcates damping threshold, i.e., EDR=1

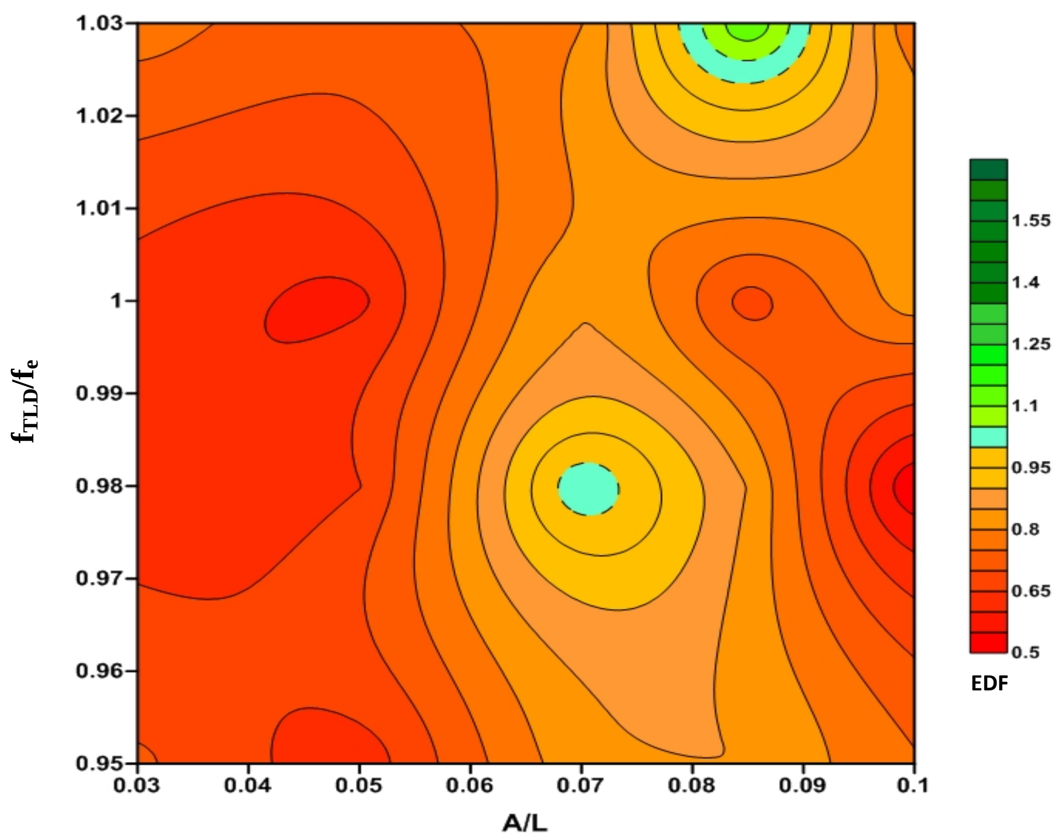


**Figure 5.3: Contour plot for energy dissipation factor at $f_{TLD}/f_s$=1.033**

### *5.4.2 Group II, $f_{TLD}/f_s$=1.093*

The effect of the external excitation frequency ratio and the amplitude-length ratio is presented in Figure 5.4 for the case of $f_{TLD}/f_s$=1.093. The corresponding contour plot of the EDF is shown in Figure 5.5.

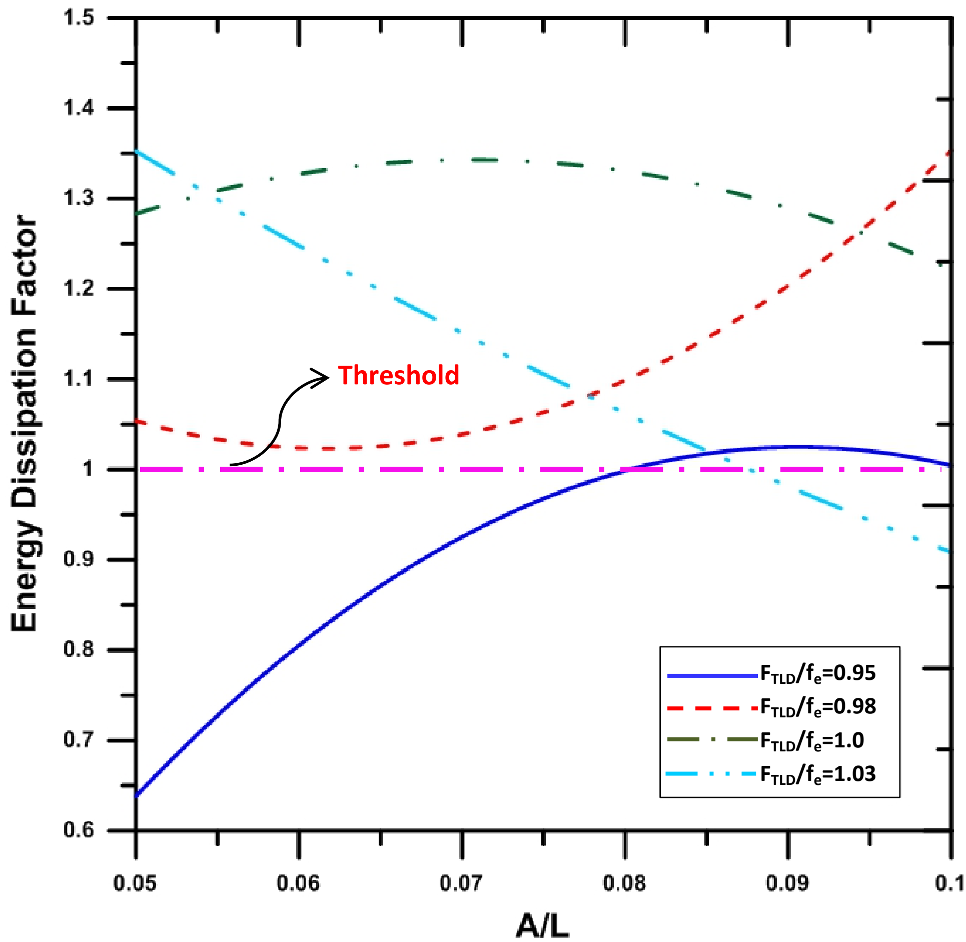


**Figure 5.4: Variation of energy dissipation factor as function of $f_{TLD}/f_e$ and A/L at $f_{TLD}/f_s$=1.093**

As illustrated in Figure 5.4, the external excitation frequency ratio of 0.98 and 1.0 are located in the damping region. This means the energy dissipation factors are greater than 1. Also, the damping effect can be found at $f_{TLD}/f_e$=1.03, but this effect is decreasing gradually until reach the amplifying region after A/L=0.088. While $f_{TLD}/f_e$=0.95 is rising slowly till reach the damping region at A/L=0.08. After all, most of these curves are greater than 1; therefore the damping effect exists at most of the external excitation frequency ratios. As shown in Figure 5.5 the damping effect is clearly observed at large area of the contour.

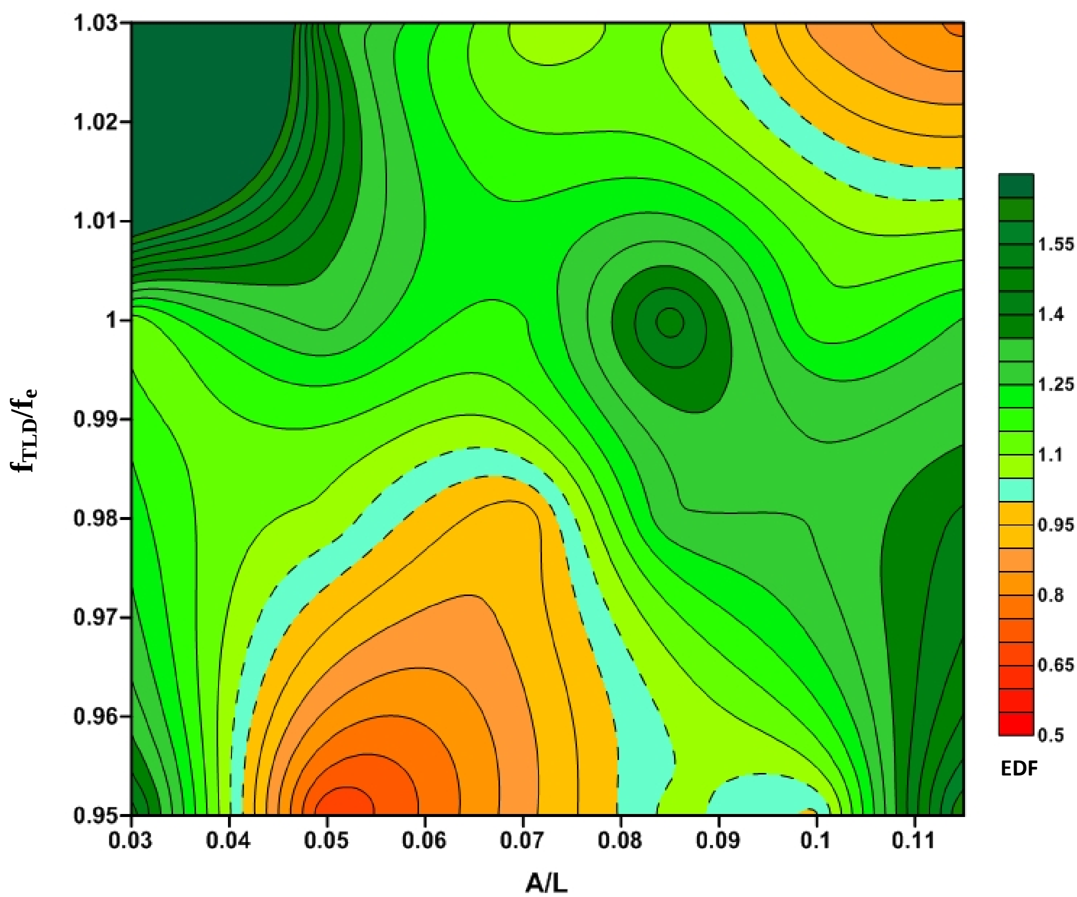


**Figure 5.5: Contour plot for energy dissipation factor at $f_{TLD}/f_s$=1.093**

### 5.4.3 *Group III, $f_{TLD}/f_s$=1.153*

Figure 5.6 exhibits the variation of energy dissipation factor at different external excitation frequency ratios at different amplitude ratio.

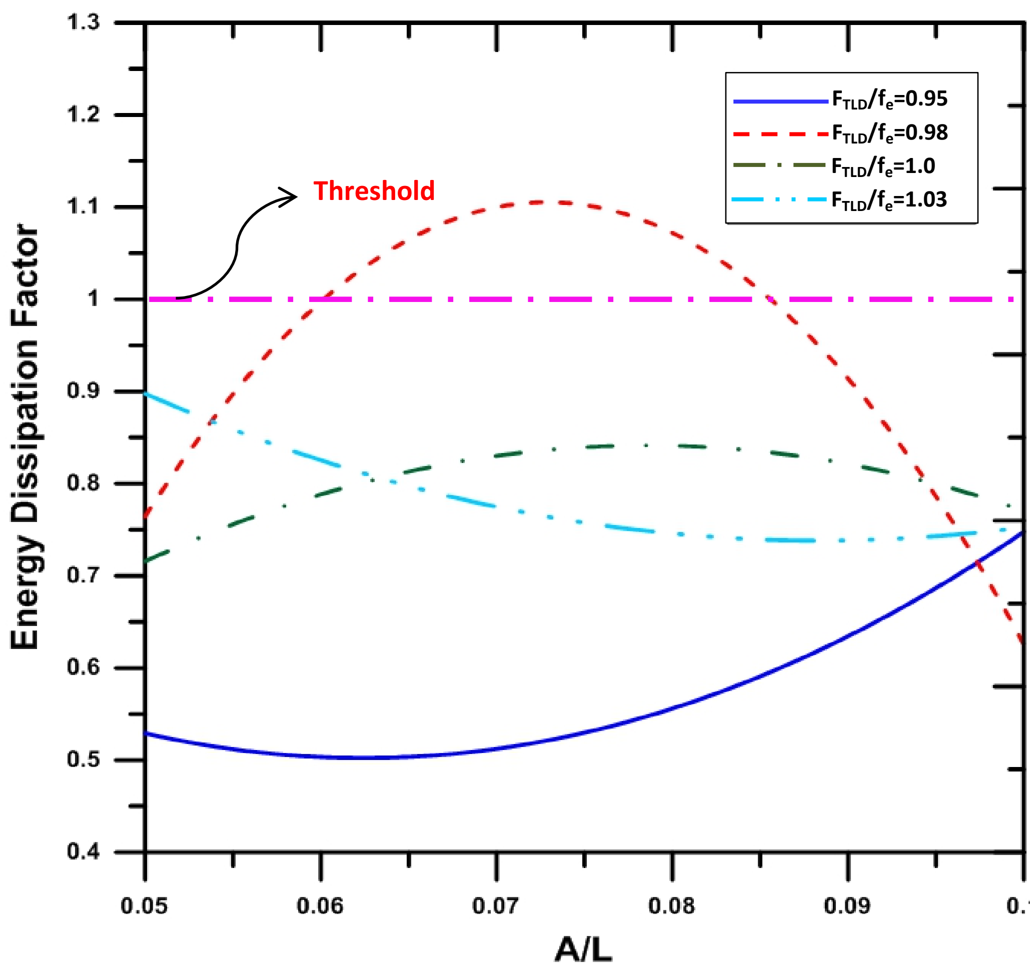


**Figure 5.6: Variation of energy dissipation factor as a factor of $f_{TLD}/f_e$ and A/L at $f_{TLD}/f_s$=1.153**

The damping was only found at $f_{TLD}/f_e$ = 0.98 between A/L= 0.06 and 0.087, while the rest of the frequency ratios are under the threshold line. For this reason, in

Figure 5.7 the red grading covers most of the area and that the damping effect does not exist at these areas.

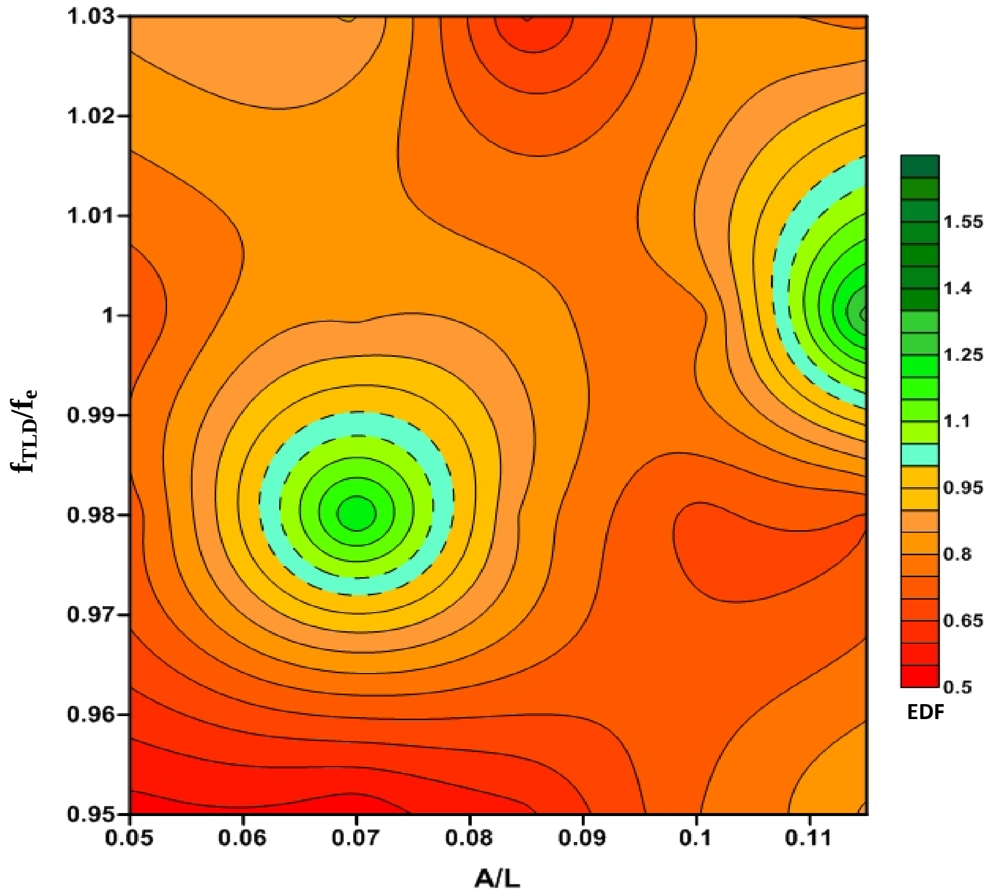


**Figure 5.7: Contour plot for energy dissipation factor at $f_{TLD}/f_s$=1.153**

## 5.5 TLD-External Excitation Frequency Ratio ($f_{TLD}/f_e$) and TLD-Structure Frequency Ratio ($f_{TLD}/f_s$) Effects at Constant Amplitude-TLD Length Ratio Effect (A/L).

The amplitude- TLD length ratio effect was investigated as a function of external excitation frequency ratio and TLD-structural frequency ratio. The contour plots below showing the damping effect at different amplitude to the TLD length ratios selected as; 0.03, 0.05, 0.07, 0.085, 0.1, and 0.115.

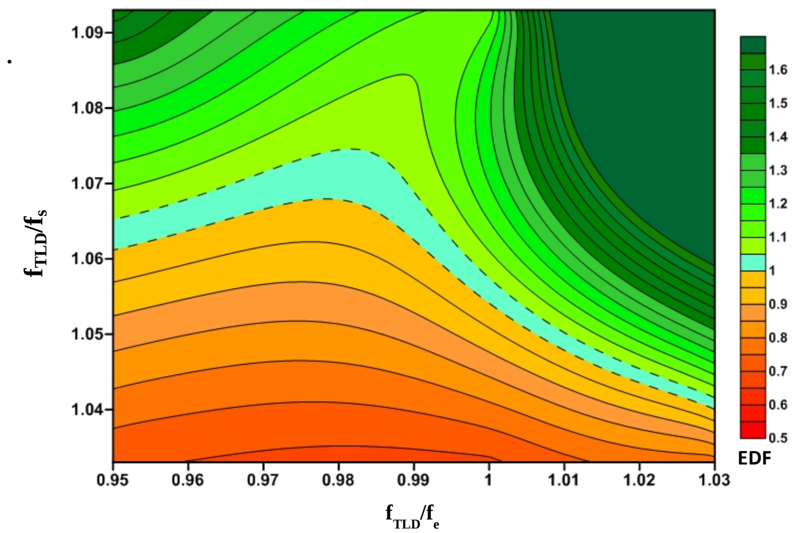


**Figure 5.8: Contour plot for energy dissipation factor at A/L=0.03**

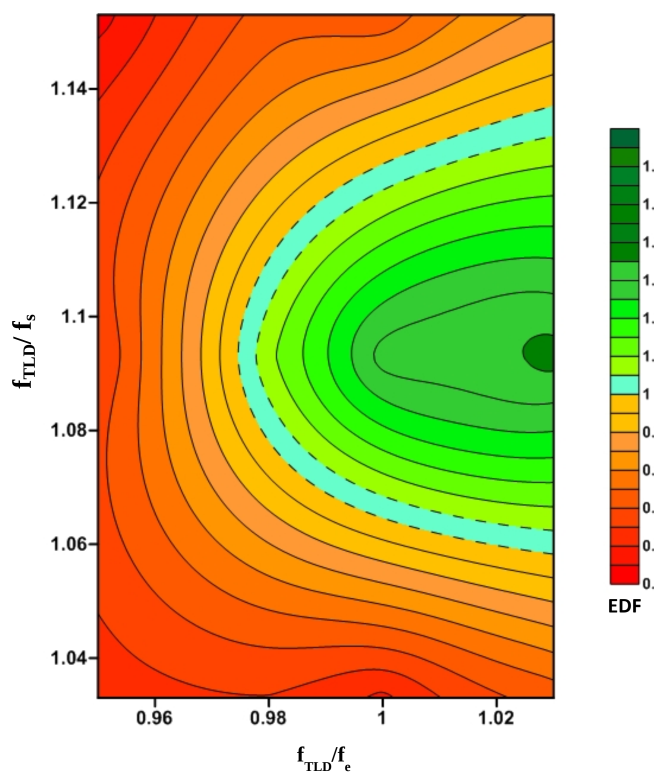


**Figure 5.9: Contour plot for energy dissipation factor at A/L=0.05**

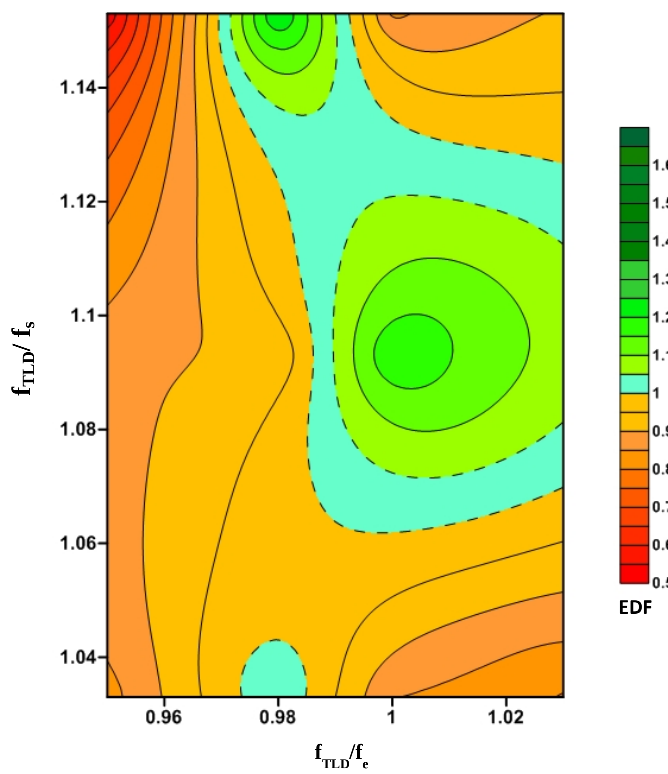


**Figure 5.10: Contour plot for energy dissipation factor at A/L=0.07**

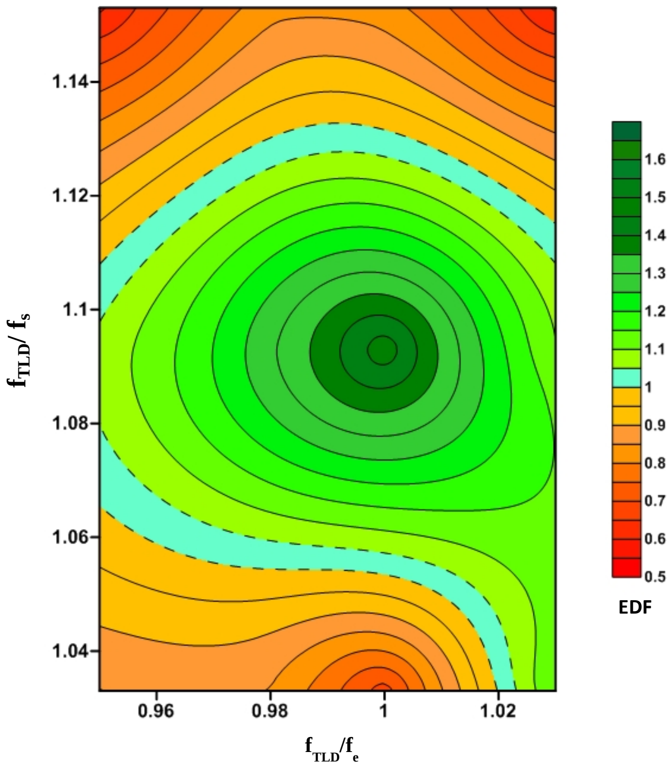


**Figure 5.11: Contour plot for energy dissipation factor at A/L=0.085**

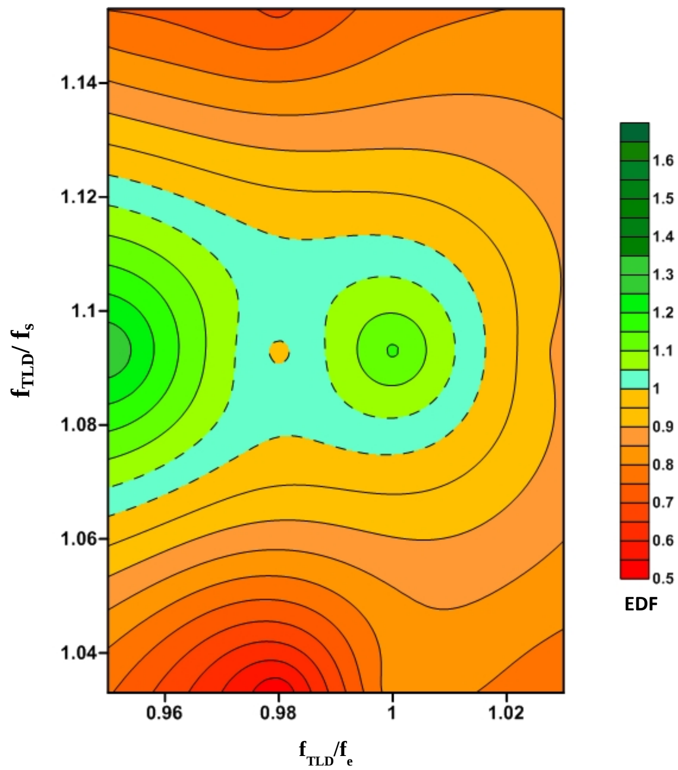


**Figure 5.12: Contour plot for energy dissipation factor at A/L=0.1**

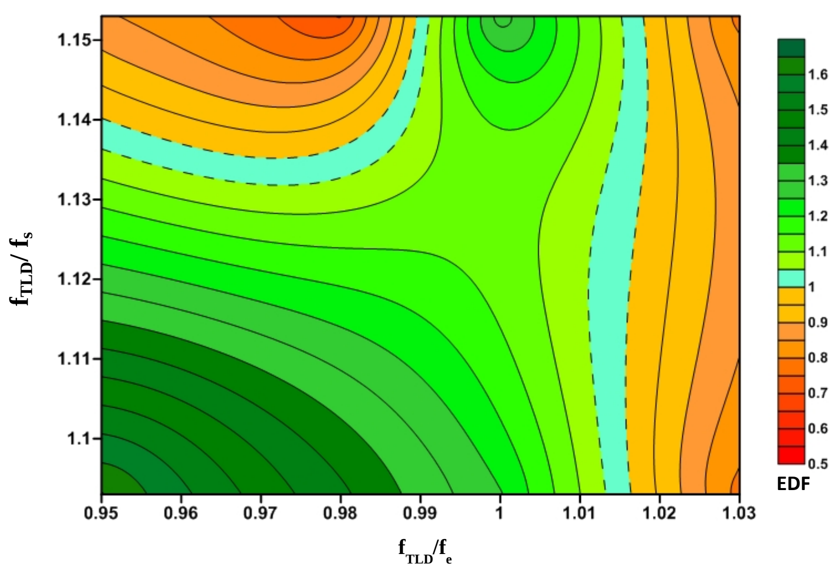


**Figure 5.13: Contour plot for energy dissipation factor at A/L=0.115**

At A/L=0.03, the damping effect can be observed between $f_{TLD}/f_s$= 1.042 and 1.093. While the amplifying effect appears between $f_{TLD}/f_s$= 1.033 and 1.065. The maximum damping effect at A/L=0.03 can be found when $f_{TLD}/f_e$ within the range of 1.01-1.03 and $f_{TLD}/f_s$ within the range of 1.06 – 1.093 as shown in Figure 5.8. In Figure 5.9, the amplifying area is larger than the damping area. However, the damping effect still exists when $0.98 \leq f_{TLD}/f_e \leq 1.03$ and $1.062 \leq f_{TLD}/f_s \leq 1.13$. At A/L=0.07, the damping effect is noticed when the energy dissipation factor within the range of 1.1-1.2 as illustrated in Figure 5.10. Similarly, the damping effect is detected when EDF within the range of 1.1-1.6 at A/L=0.085,0.115 while the damping effect at A/L=0.1 can be found at EDF= 1.1-1.3 as shown in Figures 5.11, 5.12 and 5.13, respectively.

## 5.6 TLD-Structure Frequency Ratio ($f_{TLD}/f_s$) and Amplitude-TLD Length Ratio Effect (A/L) Effects at Constant External Excitation Frequency Ratio Effect ($f_{TLD}/f_e$)

The external excitation frequency ratio effect is examined as a function of Amplitude ratio and structural natural frequency. The contour plots bellow showing the damping effect at different $f_{TLD}/f_e$.

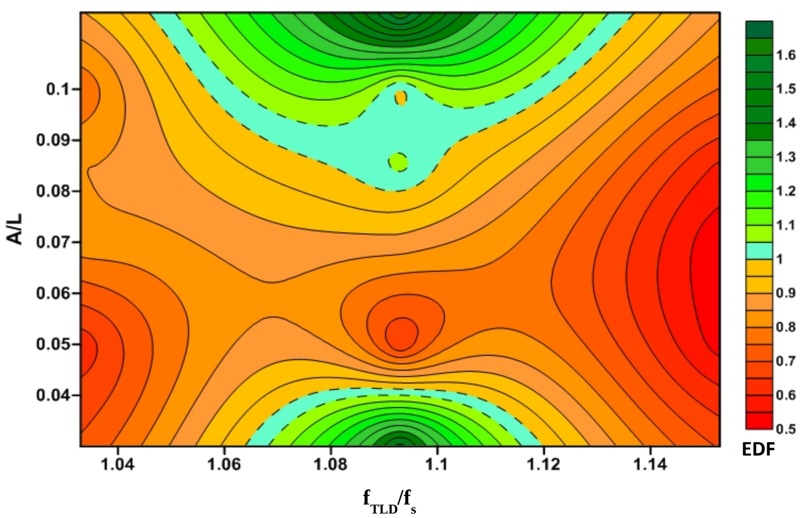


Figure 5.15: Contour plot for energy dissipation factor at $f_{TLD}/f_e$ =0.95

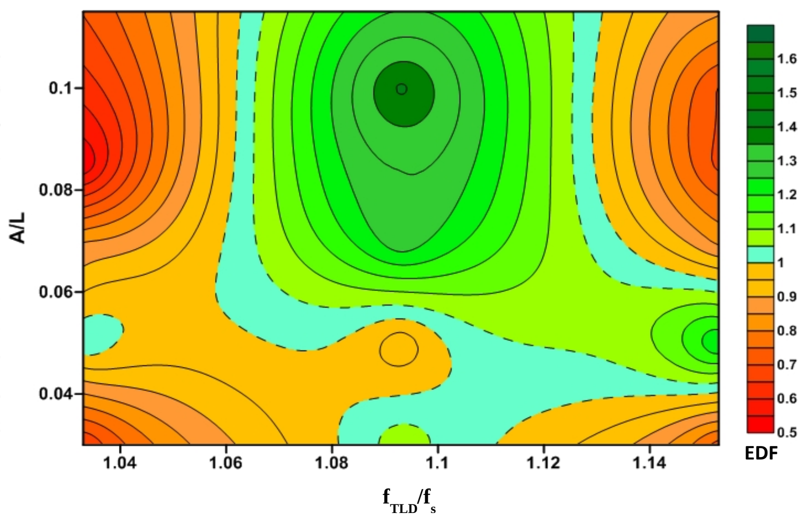


Figure 5.14: Contour plot for energy dissipation factor at $f_{TLD}/f_e$ =0.98

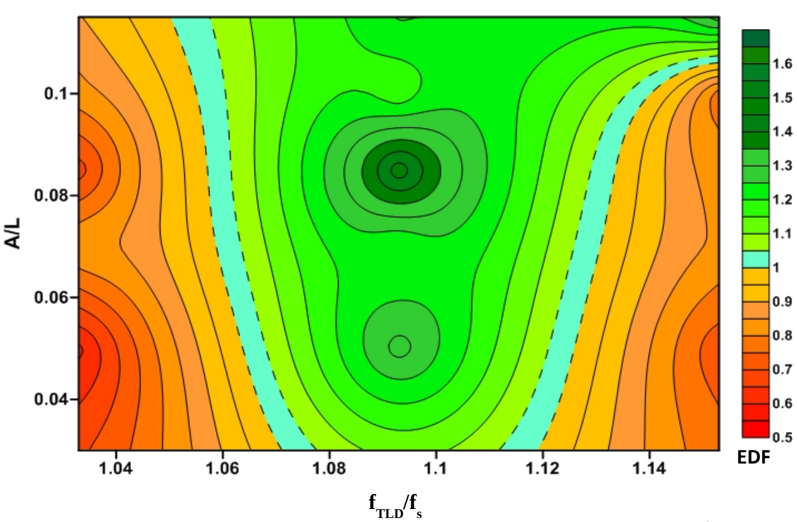


Figure 5.17 Contour plot for energy dissipation factor at $f_{TLD}/f_e$ =1.0

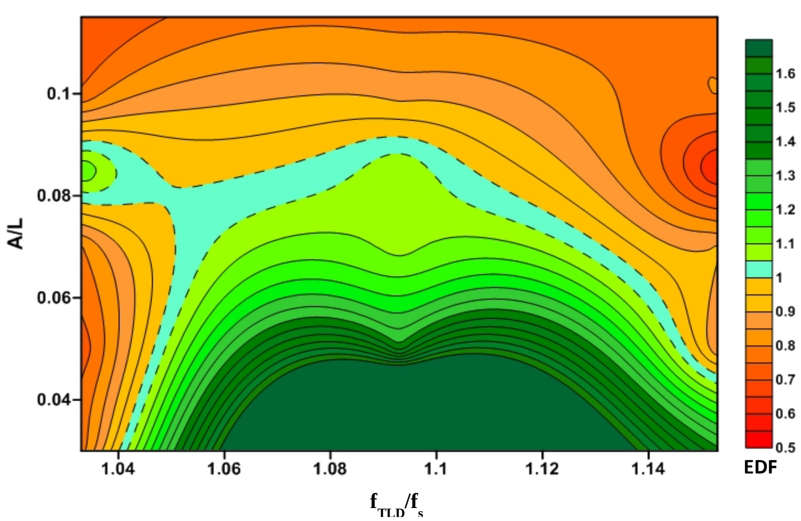


Figure 5.16: Contour plot for energy dissipation factor at $f_{TLD}/f_e$ =1.03

As shown in Figure 5.14, the damping effect appears at A/L<0.04 when $f_{TLD}/f_s$ within the range of 1.065-1.17, and at A/L>0.092 when $f_{TLD}/f_s$ within the range of 1.05-1.13. At $f_{TLD}/f_e$=0.98, the maximum damping effect can be noticed when A/L within the range of 0.093-0.11 and $f_{TLD}/f_s$ within the range of 1.09-1.1, while the maximum amplifying effect can be observed at 0.08> A/L <0.1 and $f_{TLD}/f_s$ <1.04 as presented in Figure 5.15. As can be seen in Figure 5.16, the large area is covered by the green grading and it begins when $f_{TLD}/f_s$=1.06. In the other meaning, the damping can be detected after $f_{TLD}/f_s$=1.06. The maximum damping effect can be got when $1.06 \leq f_{TLD}/f_s < 1.14$ and A/L <0.05 at $f_{TLD}/f_e$=1.03 as shown in Figure 5.17.

### 5.7 TLD Damping Correlation

Due to the nonlinear behavior of the sloshing motion inside the TLD, the damping effect depends on all three parameters considered in this study. For this reason, the following empirical equation (5.5) has been produced to correlate the TLD damping as function of $f_{TLD}/f_s$, A/L and $f_{TLD}/f_e$.

$$EDF = 53.395\left(\frac{f_{TLD}}{f_s}\right) + 123.944\left(\frac{A}{L}\right) + 106.522\left(\frac{f_{TLD}}{f_e}\right) - 84.058\left(\frac{f_{TLD}}{f_s}\right)^2 - 50.210\left(\frac{A}{L}\right)^2 - 67.409\left(\frac{f_{TLD}}{f_e}\right)^2 - 16.067\left(\frac{f_{TLD}}{f_s}\right)\left(\frac{A}{L}\right) + 32.006\left(\frac{f_{TLD}}{f_s}\right)\left(\frac{f_{TLD}}{f_e}\right) - 98.467\left(\frac{A}{L}\right)\left(\frac{f_{TLD}}{f_e}\right) - 140.488 \qquad (5.5)$$

Equation (5.5) is valid for $0.03 < \frac{A}{L} \leq 0.115$ and $0.95 < \frac{f_{TLD}}{f_e} \leq 1.03$. The maximum deviation produced by equation 5.5 is ±14.10 %.

### 5.8 Implementation of the Current Design Charts for a Real Case

The design charts (contour plots) discussed before can be used by the designer to determine the optimum design and operating parameters of a TLD. The following example illustrates how these design charts can be used: A SDOF structure is subjected to wind, which produces a sinusoidal excitation with excitation amplitude A of 0.1 m and excitation frequency $f_e$ *of* 1.0 Hz. Since the TLD showed good damping performance TLD-structure frequency ratio of 1.093, a design point can be chosen for this case, as shown in Figure 5.18.

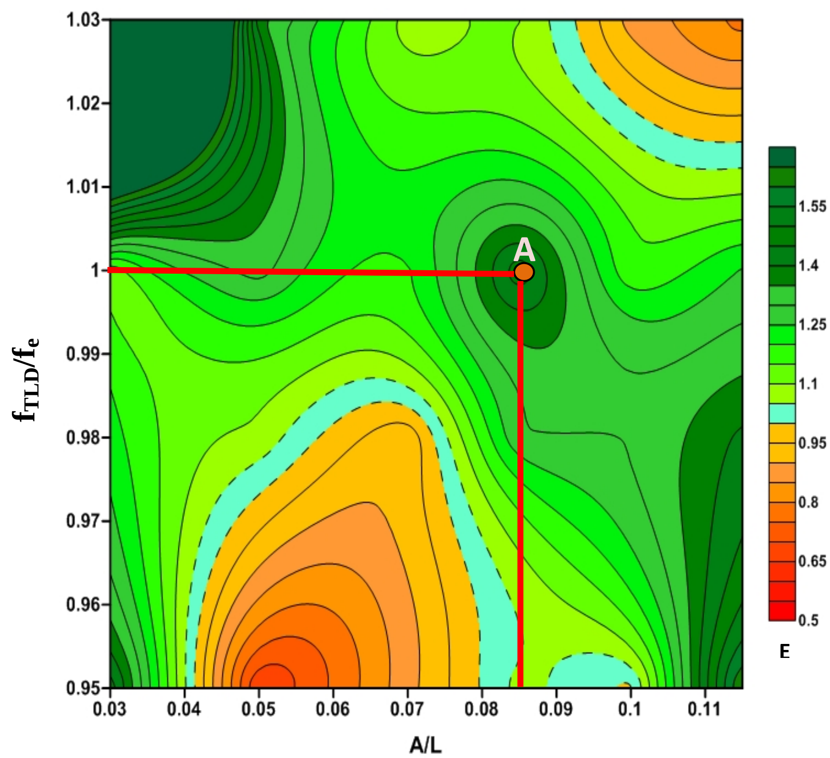


**Figure 5.18: Contour plot for energy dissipation factor at $f_w/f_s$=1.093**

**Table 5.6: TLD parameters**

| | |
|---|---|
| $f_{TLD}/f_e$=1 | $f_{TLD}$=1 HZ |
| A/L=0.085 | L=1.18 m |

Based on the selected design point, the $f_{TLD}$ and L can be calculated as shown in Table (5.6). The depth of water inside TLD can be calculated from the equation of the linear wave theory h in this case is equal 0.3m.

# 6 Chapter 6: Summary, Conclusion and Future work

## 6.1 Summary and Conclusion

TLDs can be effectively used for damping vibration due to wind loading. TLDs are effective passive dynamic absorbers that outweigh other passive damping devices due to their low cost and availability in buildings. Various numerical models have been developed to predict sloshing motion inside TLDs exposed to various external excitation forces. However, many of these models have limited applicability. An in-house numerical model has been developed by Oda (2012) to solve the full form of Navier-Stockes equations and the VOF and CSF methods without any linearization assumptions, furthermore the model can account all the dynamic stresses on free surface. The interaction of the TLD with structure has been taken into account. The response of the structure has been determined by solving the structure equation of motion using the Duhamel integral method.

A parametric study has been conducted to investigate the effect of TLD-structure frequency ratio ($f_{TLD}/f_s$), external excitation amplitude-TLD length ratio (A/L) and external excitation frequency ratio ($f_{TLD}/f_e$) on the TLD damping performance. The TLD damping performance has been evaluated using the energy dissipation ratio (EDR) and the energy dissipation factor (EDF). Results of this study have been used to develop a set of design contour plots of the TLD EDF and an empirical design correlation, which can be used to determine the optimum design and operating parameters of a TLD. The developed correlation relates the EDF to all parameters considered in this study and it has a maximum error of ±14.10 %. The use of the developed design charts have been demonstrated for an application.

## 6.2 Future work

The following are some suggestions for future work for those who are interested in the same topic:

1- The structural model considered in this study is a single degree of freedom (SDOF) structure. Extending this study to consider multi-degree of freedom structures.

2- The current numerical model is developed for two-dimensional flows. Extending the current model capability to three-dimensional would permit studying any TLD irregular geometries.

3- Developing the current correlation equation to be more accurate and lower uncertainty by studying more test cases.

## References


Akyildiz, H., and Unal, E. (2005). Experimental investigation of pressure distribution on a rectangular tank due to the liquid sloshing. *Ocean Engineering, 32*(11), 1503-1516.

Antuono, M., Colagrossi,A.,Marrone,S. and Molteni,D. (2010). Free-surface flows solved by means of SPH schemes with numerical diffusive terms. *Computer Physics Communications, 181.3:* 532-549.

Antuono, M., Bardazzi, A., Lugni, C., and Brocchini, M. (2014). A shallow-water sloshing model for wave breaking in rectangular tanks. *Journal of Fluid Mechanics, 746*, 437-465.

Antuono, M., Bouscasse, B., Colagrossi, A., and Lugni, C. (2012). Two-dimensional modal method for shallow-water sloshing in rectangular basins. *Journal of Fluid Mechanics, 700*, 419-440.

Ashgriz, N., and Poo, J. (1991). FLAIR: Flux line-segment model for advection and interface reconstruction. *Journal of Computational Physics, 93(2), 449-468.*

Babaei, R., Abdollahi, J., Homayonifar, P., Varahram, N., and Davami, P. (2006). Improved advection algorithm of computational modeling of free surface flow using structured grids. *Computer methods in applied mechanics and engineering, 195(7), 775-795.*

Banerji, P., Murudi, M., Shah, A. H., and Popplewell, N. (2000). Tuned liquid dampers for controlling earthquake response of structures. *Earthquake engineering \and structural dynamics, 29(5), 587-602.*

Bassman, M. (2000). A three dimensional model of an impacting droplet. *Ph.D. Thesis, University of Toronto, Toronto, Canada*.

Bellet, M., and Chenot, J. (1993). A Lagrangian approach to fluid flow in metal casting processes. 287-316.

Bouscasse, B., Antuono, M., Colagrossi, A., and Lugni, C. (2013). Numerical and experimental investigation of nonlinear shallow water sloshing. *Int. J. Nonlinear Sci. Numer. Simul., 14*(2), 123-138.

Bredmose, H., Brocchini, M., Peregrine, D., and Thais, L. (2003). Experimental investigation and numerical modelling of steep forced water waves. *Journal of Fluid Mechanics, 490*, 217-249.

Chan, R. K.-C., and Street, R. L. (1970). A computer study of finite-amplitude water waves. *Journal of Computational Physics, 6*(1), 68-94.

Chang, C., and Gu, M. (1999). Suppression of vortex-excited vibration of tall buildings using tuned liquid dampers. *Journal of Wind Engineering and Industrial Aerodynamics, 83*(1), 225-237.

Chen, W., Haroun, M. A., and Liu, F. (1996). Large amplitude liquid sloshing in seismically excited tanks. *Earthquake engineering \and structural dynamics, 25*(7), 653-669.

Colagrossi, A., Palladino, F., Greco, M., Lugni, C., and Faltinsen, O. (2006). Experimental and numerical investigation of 2D sloshing: scenarios near the critical filling depth.

Dalrymple, R. A., and Dean, R. G. (1991). *Water wave Mechanics for Engineers and Scientists.* Prentice-Hall.

Delorme, L., Colagrossi, A., Souto-Iglesias, A., Zamora-Rodriguez, R., and Botia-Vera, E. (2009). A set of canonical problems in sloshing, Part I: Pressure field in forced roll—comparison between experimental results and SPH. *Ocean Engineering, 36*(2), 168-178.

Faltinsen, O. M. (1978). A numerical nonlinear method of sloshing in tanks with two-dimensional flow. *Journal of Ship Research*, *22*(3).

Faltinsen, O. M. (2005). *Hydrodynamics of high-speed marine vehicles.* Cambridge university press.

Faltinsen, O. M., and Timokha, A. N. (2002). Asymptotic modal approximation of nonlinear resonant sloshing in a rectangular tank with small fluid depth. *Journal of Fluid Mechanics, 470*, 319-357.

Faltinsen, O. M., Rognebakke, O. F., Lukovsky, I. A., and Timokha, A. N. (2000). Multidimensional modal analysis of nonlinear sloshing in a rectangular tank with finite water depth. *Journal of Fluid Mechanics, 407*, 201-234.

Fang, J., Parriaux, A., Rentschler, M., and Ancey, C. (2009). Improved SPH methods for simulating free surface flows of viscous fluids. *Applied Numerical Mathematics, 59*(2), 251-271.

Floryan, J., and Rasmussen, H. (1989). Numerical methods for viscous flows with moving boundaries. *Applied Mechanics Reviews, 42*(12), 323-341.

Frandsen, J. (2005). Numerical predictions of tuned liquid tank structural systems. *Journal of Fluids and Structures, 20*(3), 309-329.

Frandsen, J. B. (2004). Sloshing motions in excited tanks. *Journal of Computational Physics, 196*(1), 53-87.

Frandsen, J., and Borthwick, A. (2003). Simulation of sloshing motions in fixed and vertically excited containers using a 2-D inviscid $\sigma$-transformed finite difference solver. *Journal of Fluids and Structures, 18*(2), 197-214.

Fujino, PACHECO, B. M., and CHAISERI, P. (1988). Parametric studies on tuned liquid damper (TLD) using circular containers by free-oscillation experiments. *Structural Engineering/Earthquake Engineering, 19*(2), 381s-391s.

Fujino, Y., Sun, L., Pacheco, B. M., and Chaiseri, P. (1992). Tuned liquid damper (TLD) for suppressing horizontal motion of structures. *Journal of Engineering Mechanics, 118*(10), 2017-2030.

Hamed, M., and Floryan, J. (1998). Numerical simulation of unsteady nonisothermal capillary interfaces. *Journal of computational physics, 145*(1), 110-140.

Hamelin, J. (2007). The effect of screen geometry on the performance of a tuned liquid damper.

Harlow, F. H., Welch, J. E., and others. (1965). Numerical calculation of time-dependent viscous incompressible flow of fluid with free surface. *Physics of fluids, 8*(12), 2182.

Hill, D. F. (2003). Transient and steady-state amplitudes of forced waves in rectangular basins. *Physics of Fluids (1994-present), 15*(6), 1576-1587.

Hirt, C. W., and Nichols, B. D. (1981). Volume of fluid (VOF) method for the dynamics of free boundaries. *Journal of computational physics, 39*(1), 201-225.

Iglesias, A. S., Rojas, L. P., and Rodriguez, R. Z. (2004). Simulation of anti-roll tanks and sloshing type problems with smoothed particle hydrodynamics. *Ocean Engineering, 31*(8), 1169-1192.

Kaneko, S., and Ishikawa, M. (1999). Modeling of tuned liquid damper with submerged nets. *Journal of pressure vessel technology, 121*(3), 334-343.

Kareem, A., Kijewski, T., and Tamura, Y. (1999). Mitigation of motions of tall buildings with specific examples of recent applications. *Wind and structures, 2*(3), 201-251.

Kim, M. S., and Lee, W. I. (2003). A new VOF-based numerical scheme for the simulation of fluid flow with free surface. Part I: New free surface-tracking algorithm and its verification. *International Journal for Numerical Methods in Fluids, 42*(7), 765-790.

Koh, C., Mahatma, S., and Wang, C. (1994). Theoretical and experimental studies on rectangular liquid dampers under arbitrary excitations. *Earthquake engineering and structural dynamics, 23*(1), 17-31.

Kothe, D., Rider, W., Mosso, S., Brock, J., and Hochstein, J. (1996). Volume tracking of interfaces having surface tension in two and three dimensions. *AIAA paper, 96*(0859), 1-18.

Lemos, C. (1992). Wave breaking: A numerical study. *Lecture notes in Engineering*.

Lepelletier, T., and Raichlen, F. (1988). Nonlinear oscillations in rectangular tanks. *Journal of Engineering Mechanics, 114*(1), 1-23.

Li, H.-N., Jia, Y., and Wang, S.-Y. (2004). Theoretical and experimental studies on reduction for multi-modal seismic responses of high-rise structures by tuned liquid dampers. *Journal of Vibration and Control, 10*(7), 1041-1056.

Li, S., Li, G., Tang, J., and Li, Q. (2002). Shallow rectangular TLD for structural control implementation. *Applied Acoustics, 63*(10), 1125-1135.

Lin, P. (2007). A fixed-grid model for simulation of a moving body in free surface flows. *Computers and fluids, 36*(3), 549-561.

Liu, P. L., and Lin, P. (1997). A Numerical Model for Breaking Waves: The Volume of Fluid Method.

Lugni, C., Brocchini, M., and Faltinsen, O. (2006). Wave impact loads: The role of the flip-through. *Physics of Fluids (1994-present), 18*(12), 122101.

Lugni, C., Brocchini, M., and Faltinsen, O. (2010). Evolution of the air cavity during a depressurized wave impact. II. The dynamic field. *Physics of Fluids (1994-present), 22*(5), 056102.

Marivani M, Hamed MS. (2009). Numerical Simulation of Structure Response Outfitted with a Tuned Liquid Damper. Computers and Structures. *87(17-18):1154*-1165.

McKee, S., Tome, M., Ferreira, V., Cuminato, J., Castelo, A., Sousa, F., and Mangiavacchi, N. (2008). The MAC method. *Computers and Fluids, 37*(8), 907-930.

Modi, V., and Seto, M. (1997). Suppression of flow-induced oscillations using sloshing liquid dampers: analysis and experiments. *Journal of wind engineering and industrial aerodynamics, 67*, 611-625.

Modi, V., and Welt, F. (1987). Vibration Control using Nutation Dampers. *International Conference of Flow Induced Vibrations*, 369-376.

Monaghan, J. J. (1988). An introduction to SPH. *Computer physics communications, 48*(1), 89-96.

Nakayama, T. (1983). Boundary element analysis of nonlinear water wave problems. *International Journal for Numerical Methods in Engineering, 19*(7), 953-970.

Nakayama, T., and Washizu, K. (1981). The boundary element method applied to the analysis of two-dimensional nonlinear sloshing problems. *International Journal for Numerical Methods in Engineering, 17*(11), 1631-1646.

Nichols, B., Hirt, C., and Hotchkiss, R. (1980). SOLA-VOF: A solution algorithm for transient fluid flow with multiple free boundaries.

Noji, T. Y., and Hagiuda, H. (1988). Study on Vibration Control Damper Utilizing Sloshing of Water. *Journal of Wind Engineering, 37*, 557-566.

Oda T, Hamed MS, and Ghani S. (2012). On Wave Breaking inside Tuned Liquid Dampers. Proceedings. *The 9th International Conference on Heat Transfer, Fluid Mechanics and Thermodynamics,Malta,2012-07-16*

Oda T. F., Hamed M.S., and Ghani S. (2013), On the Damping of Wind–Induced Vibration in Tall Buildings. *The Fourteenth International Conference on Civil, Structural and Environmental Engineering Computing, Italy Sep 2013.*

Oda T. F., Hamed M.S., and Ghani S., (2014).Numerical Study of the Effect of Liquid Sloshing Inside TLD on Suppression of Gust Wind- Induced Vibration in High Rise Buildings. *HEAFAT 2014, 14-16 July 2014, Orlando, Florida, USA.*

Okamoto, T., and Kawahara, M. (1990). Two-dimensional sloshing analysis by Lagrangian finite element method. *International Journal for Numerical Methods in Fluids*, *11*(5), 453-477.

Panigrahy, P., Saha, U., and Maity, D. (2009). Experimental studies on sloshing behavior due to horizontal movement of liquids in baffled tanks. *Ocean Engineering, 36*(3), 213-222.

Ramaswamy, B., Kawahara, M., and Nakayama, T. (1986). Lagrangian finite element method for the analysis of two-dimensional sloshing problems. *International Journal for Numerical Methods in Fluids, 6*(9), 659-670.

Reed, D., Yu, J., Yeh, H., and Gardarsson, S. (1998). Investigation of tuned liquid dampers under large amplitude excitation. *Journal of Engineering Mechanics, 124*(4), 405-413.

Rider, W. J., and Kothe, D. B. (1998). Reconstructing volume tracking. *Journal of computational physics, 141*(2), 112-152.

Rudman, M. (1997). Volume-tracking methods for interfacial flow calculations. *International journal for numerical methods in fluids, 24*(7), 671-691.

Scardovelli, R., and Zaleski, S. (1999). Direct numerical simulation of free-surface and interfacial flow. *Annual review of fluid mechanics, 31*(1), 567-603.

Shimizu, T., and Hayama, S. (1987). Nonlinear responses of sloshing based on the shallow water wave theory. *JSME international journal, 30*(263), 806-813.

Siddique, M., Hamed, M., and El Damatty, A. (2005). A nonlinear numerical model for sloshing motion in tuned liquid dampers. *International Journal of Numerical Methods for Heat and Fluid Flow, 15*(3), 306-324.

Soo Kim, M., Sun Park, J., and Lee, W. I. (2003). A new VOF-based numerical scheme for the simulation of fluid flow with free surface. Part II: application to the cavity filling and sloshing problems. *International journal for numerical methods in fluids, 42*(7), 791-812.

Soong, T., and Dargush, G. (1997). *Passive energy dissipation systems in structural engineering, 1997.* John Wiley and Soms Ltda.

Souto-Iglesias, A., Delorme, L., Perez-Rojas, L., and Abril-Perez, S. (2006). Liquid moment amplitude assessment in sloshing type problems with smooth particle hydrodynamics. *Ocean Engineering, 33*(11), 1462-1484.

Sun, L., and Fujino, Y. (1994). A semi-analytical model for tuned liquid damper (TLD) with wave breaking. *Journal of Fluids and Structures, 8*(5), 471-488.

Sun, L., Fujino, Y., Chaiseri, P., and Pacheco, B. (1995). The properties of tuned liquid dampers using a TMD analogy. *Earthquake engineering \and structural dynamics, 24*(7), 967-976.

Sun, L., Fujino, Y., Pacheco, B., and Chaiseri, P. (1992). Modelling of tuned liquid damper (TLD). *Journal of Wind Engineering and Industrial Aerodynamics*, *43*(1), 1883-1894.

T., O., and Fujii, K. (1989). A Boundary Element Analysis for Two dimentional Nonlinear Sloshing Problem. *Structural Engineering, 35A*, 575-584.

Tait, M. J. (2004). The Performance of 1-D and 2-D Tuned Liquid Dampers. *Ph.D. Thesis, University of Western Ontario, Canada*.

Tait, M., El Damatty, A., Isyumov, N., and Siddique, M. (2005). Numerical flow models to simulate tuned liquid dampers (TLD) with slat screens. *Journal of Fluids and Structures, 20*(8), 1007-1023.

Tamura, Y., Fujii, K., Ohtsuki, T., Wakahara, T., and Kohsaka, R. (1995). Effectiveness of tuned liquid dampers under wind excitation. *Jornal of Engineering Structures, 17*(9), 609-621.

Tavakoli, R., Babaei, R., Varahram, N., and Davami, P. (2006). Numerical simulation of liquid/gas phase flow during mold filling. *Computer methods in applied mechanics and engineering*, *196*(1), 697-713.

Thé J.L., R. G. (1994). Surface adaptive final volume method for solving free surface flows. *Numerical Heat Transfer, 26(B),* 367-80.

Torrey, M. D., Cloutman, L. D., Mjolsness, R. C., and Hirt, C. (1985). NASA-VOF2D: A computer program for incompressible flows with free surfaces.

Wakahara, T., Ohyama, T., and Fujii, K. (1992). Suppression of wind-induced vibration of a tall building using tuned liquid damper. *Journal of Wind Engineering and Industrial Aerodynamics, 43*(1), 1895-1906.

Warnitchai, P., and Pinkaew, T. (1998). Modelling of liquid sloshing in rectangular tanks with flow-dampening devices. *Engineering Structures, 20*(7), 593-600.

Wu, G., Ma, Q., and Taylor, R. E. (1998). Numerical simulation of sloshing waves in a 3D tank based on a finite element method. *Applied Ocean Research, 20*(6), 337-355.

Yamamoto, K., and Kawahara, M. (1999). Structural oscillation control using tuned liquid damper. *Computers and structures, 71*(4), 435-446.

Zang, Y., Xue, S., and Kurita, S. (2000). A boundary element method and spectral analysis model for small-amplitude viscous fluid sloshing in couple with structural vibrations. *International journal for numerical methods in fluids*, *32*(1), 69-83.